Geochemical Perspectives Letters

Warm Archean oceans reconstructed from oxygen isotope composition of early-life remnants

R. Tartèse*[1,2], M. Chaussidon[3], A. Gurenko[4], F. Delarue[1], F. Robert[1]

OPEN ACCESS

doi: 10.7185/geochemlet.1706

Abstract

Deciphering the surface conditions on the Earth during Archean times (> 2.5 billion years ago – Ga) is crucial to constrain the conditions that promoted the development of life. The progressive shift through time of the oxygen isotopic compositions of Precambrian siliceous sediments – the so-called cherts – has been interpreted as indicating a secular decrease of seawater temperature by 50-80 °C from the early Archean to the present-day. However, this interpretation has been questioned, notably because it assumes that the seawater oxygen isotopic composition has remained globally constant since 3.5 Ga, though this has never been tested by direct isotopic measurements on Archean samples. Here we report measurements of the oxygen isotopic composition of carbonaceous matter indigenous to Precambrian cherts up to *ca.* 3.5 Ga. These new results demonstrate that the oxygen isotope composition of seawater during most of the Precambrian remained around 0 ± 5 ‰, which is consistent with the composition of present day seawater. Combined with the chert oxygen isotope composition record, this indicates that *ca.* 3.5 Ga ago ocean bottom-water temperatures were ~50-60 °C higher than today.

Received 13 July 2016 | Accepted 17 September 2016 | Published 18 October 2016

Introduction

The oxygen isotopic composition (hereafter reported in ‰ using the delta notation, $\delta^{18}O_{sample} = [(^{18}O/^{16}O)_{sample}/(^{18}O/^{16}O)_{SMOW} - 1] \times 1000$ where SMOW stands for the present day Standard Mean Ocean Water composition) of cherts has increased systematically during the last 3.5 Ga from ~20 ‰ to ~35 ‰ (Knauth

1. Institut de Minéralogie, de Physique des Matériaux et de Cosmochimie (IMPMC), Sorbonne Universités, UPMC Univ Paris 06, MNHN, CNRS, IRD, 75005 Paris, France
2. Department of Physical Sciences, The Open University, Walton Hall, MK7 6AA Milton Keynes, United Kingdom
* Corresponding author (email: romain.tartese@mnhn.fr)
3. Institut de Physique du Globe de Paris (IPGP), Université Sorbonne-Paris-Cité, CNRS UMR 7154, 75238 Paris Cedex 05, France
4. Centre de Recherches Pétrographiques et Géochimiques, UMR 7358, Université de Lorraine, 54501 Vandoeuvre-lès-Nancy, France

and Epstein, 1976; Knauth and Lowe, 2003; Robert and Chaussidon, 2006). Based on the temperature-dependence of the oxygen isotopic fractionation between silica and water (Knauth and Epstein, 1976), this isotopic record implies that the formation temperature (*T*) of cherts decreased by 50-80 °C since Archean times, assuming that silica formed from water with a $\delta^{18}O$ of ~0 ‰ (Knauth and Epstein, 1976; Knauth and Lowe, 2003; Robert and Chaussidon, 2006). While this assumption is consistent with $\delta^{18}O$ values measured in *ca.* 3.8 Ga ophiolites (Pope *et al.*, 2012) and with geochemical models indicating that $\delta^{18}O_{seawater}$ is buffered to around 0 ± 2 ‰ within a few tens of million years (*e.g.*, Lécuyer and Allemand, 1999), this hypothesis of a near constant $\delta^{18}O_{seawater}$ through time has never been tested by direct measurements on Precambrian samples.

Several arguments have been put forward challenging the interpretation of elevated surface *T* during Precambrian times. Isotopic exchange during diagenesis and chert alteration could have decreased the original $\delta^{18}O_{chert}$, for example. However, observations of large ranges of $\delta^{18}O_{chert}$ values at the micrometre scale in individual quartz grains (*e.g.*, Marin-Carbonne *et al.*, 2012) showed that Precambrian cherts can preserve a record of their pristine O-isotope signature, with diagenetic effects resulting in a limited excess of ~15-20 °C on the crystallisation *T* calculated previously. Also, the chert O-isotope record of warm *T* during the Precambrian apparently conflicts with evidence for large scale glaciations, such as the 2.2-2.45 Ga Huronian glaciations (*e.g.*, Evans *et al.*, 1997; Young, 2014). Therefore, it has been argued that constraints for a constant $\delta^{18}O_{seawater}$ over time were indirect and weak, and that the increase of $\delta^{18}O_{chert}$ values since 3.5 Ga rather reflects a 10-15 ‰ increase of $\delta^{18}O_{seawater}$, with average surface *T* remaining around 15-30 °C (*e.g.*, Kasting *et al.*, 2006; Jaffrés *et al.*, 2007). To provide further constraints on this key issue, we have investigated chert-hosted biogenic carbonaceous remnants, whose O isotope composition is directly related to that of the water in which their precursor microorganisms thrived.

The isotopic composition of biomolecules is largely determined by metabolic exchange between living organisms and their environment. In aquatic heterotrophic organisms, for example, *ca.* 70-80 % of organic matter-derived oxygen originates from water (see Supplementary Information). In living organisms, fractionation of O isotopes between water and organic compounds results from both equilibrium and kinetic processes (*e.g.*, Schmidt *et al.*, 2015). As a result, different organic compounds are characterised by different O isotope compositions: oxygen is enriched in ^{18}O by ~27 ± 5 ‰ compared to ambient water in carbohydrates such as cellulose, while it is enriched by ~19 ± 3 ‰ in carboxyl groups, for example (*e.g.*, Schmidt *et al.*, 2015). Chemical changes occurring during thermal maturation of organic matter (OM) may alter O isotope compositions of various organic compounds. O-rich thermolabile components (*e.g.*, carbohydrates and amino acids) are quickly degraded during maturation, resulting in residual OM (kerogen) dominated by resistant aromatic moieties in which O is mostly bound in hydroxyl (–OH), ketone (–C=O) and carboxyl (–COOH) functional groups (*e.g.*, De Gregorio *et al.*, 2011). Proto-kerogens derived from marine algae collected in recent surface sediments and isolated from Lower

Jurassic Toarcian shales are characterised by $\delta^{18}O$ values that are on average 20.5 ± 1.1 ‰ (2 SD) higher than the O isotope composition of waters in which the precursor biomass thrived (Supplementary Information). Such a $\Delta^{18}O_{kerogen\text{-}water}$ is similar to our previous estimates (Tartèse *et al.*, 2016) and indicates that the O isotope composition of bulk immature kerogens is consistent with that of O bound to carboxyl functional groups, which appear to be one of the more resistant O-bearing functional group in thermally altered OM (*e.g.*, De Gregorio *et al.*, 2011). This suggests that oxygen in sedimentary OM preserves the $\delta^{18}O$ signature of the carboxyl functional groups of its precursor biomass, which does not seem to be fractionated during maturation. Biogenic carbonaceous remnants have, therefore, a great potential to provide direct constraints on the O isotope composition of waters in which their precursor biomass lived.

Oxygen Isotope Composition of Precambrian Kerogens

Bulk pyrolysis results obtained on 18 kerogens isolated from Precambrian cherts up to *ca.* 3.5 Ga have consistent $\delta^{18}O$ values clustering around 20 ± 5 ‰ (Wedeking, 1983) (Fig. 1 and Table S-1). To provide further constraints on the significance of bulk kerogen $\delta^{18}O$ values, we used Secondary Ion Mass Spectrometry (SIMS) to analyse additional kerogens isolated by acid-maceration from cherts ranging in age from 0.58 to 3.42 Ga and affected by metamorphic conditions no higher than those of lower greenschist facies (Delarue *et al.*, 2016) (Supplementary Information). Bulk C isotope compositions of these kerogens are compatible with typical biological signatures ($\delta^{13}C$ between -35 and -25 ‰; Fig. 1). Most kerogens have average SIMS $\delta^{18}O$ values between *ca.* 15 and 25 ‰, which is consistent with values obtained by pyrolysis on bulk kerogens (Fig. 1). The kerogens older than 3.0 Ga analysed by SIMS have strikingly consistent average $\delta^{18}O$ values between 19.5 ± 3.2 and 22.7 ± 3.9 ‰ (Table 1). In contrast, a few Proterozoic kerogens display large deviations from these older samples, with $\delta^{18}O$ values ranging from 4.2 ± 3.0 ‰ for the 1.88 Ga Gunflint samples to 28.5 ± 3.1 ‰ for the 1.5 Ga Jixian sample (Table 1). Other samples, such as Bitter Springs (0.8 Ga), also display a low average $\delta^{18}O$ value (8.6 ± 3.7 ‰), while average $\delta^{18}O$ values of *ca.* 25 ± 5 ‰ for the Naberru (1.85 Ga) and McArthur (1.6 Ga) kerogens are consistent within errors with those of Archean kerogens (Table 1). Finally, the average $\delta^{18}O$ of 17.0 ± 4.3 ‰ for the Ediacaran (0.58 Ga) Doushantuo kerogen is similar to the O isotope composition previously obtained for the Silurian Zdanow kerogen of 15.3 ± 1.2 ‰ (Tartèse *et al.*, 2016). For Bitter Springs kerogens, the $\delta^{18}O$ values obtained by SIMS (8.6 ± 3.7 ‰) and by pyrolysis (17.3 ± 0.6 ‰ and 17.5 ± 0.6 ‰) on kerogen residues isolated from two different samples are not consistent with each other. This may indicate that these two Bitter Springs samples correspond to slightly different time periods and/or deposition environments, for example, which can only be thoroughly assessed with further petro-geochemical investigation.

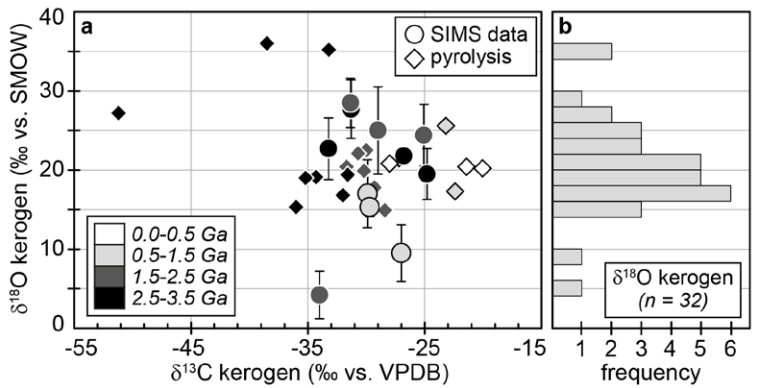

Figure 1 **(a)** Oxygen isotope compositions of the kerogens analysed by SIMS and by pyrolysis plotted against their C isotope compositions. **(b)** Frequency distribution of the measured kerogen $\delta^{18}O$ values.

The SIMS $\delta^{18}O$ values for individual kerogens vary by ~10-15 ‰ at the 20-30 µm spot scale (Fig. S-1 and Table S-2). This variability, and the variations of the measured C, O, S and Fe intensities (Fig. S-2), are similar to the variability observed for Phanerozoic kerogens (Tartèse *et al.*, 2016). It is also comparable with the variations of 5-10 ‰ observed at the micrometre scale for C isotope ratios in Precambrian microfossils (*e.g.*, Williford *et al.*, 2013). For each sample, individual $\delta^{18}O$ values display unimodal Gaussian distributions around their mean value (Fig. S-1), showing that there is no analytical evidence for multiple organic O-bearing components with variable O isotope compositions in the kerogens. The good consistency between combustion and SIMS average $\delta^{18}O$ values obtained on selected samples (Table 1) indicates that most of the SIMS $\delta^{18}O$ variability at the sample scale can be assigned to analytical effects (*e.g.*, sample topography, sputtering of mineral micro-inclusions; see Supplementary Information). This allows us to use both bulk kerogen pyrolysis and average SIMS $\delta^{18}O_{kerogen}$ values (and their standard deviation) to estimate the O isotope composition of water coeval with the kerogen precursor biomass.

The last point to consider is the possible effects of diagenesis and metamorphism on preservation of the $\delta^{18}O_{kerogen}$ values through time. During heating, kerogen loses O (and other heteroatoms such as N) as H_2O, CO and CO_2, which could in theory lead to enrichment in ^{18}O in the residual kerogen due to preferential loss of molecules containing light ^{16}O. The bulk kerogens analysed by Wedeking (1983) are up to *ca.* 3.5 billion years old and have large ranges of H/C ratios (from 0.1 to 1.4) and O contents (0.3-18.4 wt. %) (Table S-1). In these samples, $\delta^{18}O_{kerogen}$ values are neither correlated with O contents nor with H/C ratios (Fig. S-3). Therefore, there is no evidence that $\delta^{18}O$ values measured in the majority of the kerogens have been significantly altered during diagenesis and low grade metamorphism. As indicated previously, analysis of three recent

kerogens yielded a $\Delta^{18}O_{kerogen\text{-}water}$ of 20.5 ± 1.1 ‰ (Wedeking, 1983). The possible effect of temperature on biochemical O isotope fractionation is uncertain and debated (*e.g.*, Roden and Ehleringer, 2000; Sternberg and Ellsworth, 2011), and this could introduce an additional uncertainty of *ca.* ±2-3 ‰ on the O isotope composition of OM precursors. Therefore, we used a $\Delta^{18}O_{kerogen\text{-}water}$ of 20 ± 4 ‰ to calculate $\delta^{18}O_{water}$ from kerogen O isotope compositions.

Table 1 Main characteristics of the studied samples. $\delta^{13}C$ and the $\delta^{18}O$ values are given relative to VPDB and SMOW, respectively. See Supplementary Information for details and references.

Sample	Reference	Age (Ga)	Location	$\delta^{18}O_{SIMS}$ (‰)	$\delta^{18}O_{TC/EA\text{-}IRMS}$ (‰)	$\delta^{13}C$ (‰)
Doushantuo	1a of 8/25/83	0.58	Doushantuo Fm., Yangtze Gorges, South China	17.0 ± 4.3	15.0 ± 0.1	-29.9
Bitter Springs	3 of 11/2/90	0.80	Bitter Springs Fm., Amadeus Basin, Australia	8.6 ± 3.7	–	-27.0
Jixian	1 of 8/14/83	1.50	Gaoyuzhuang Group, Jixian section, North China Block, China	28.5 ± 3.1	–	-31.4
McArthur	7 of 6/21/90	1.60	McArthur Basin, Northern Territory, Australia	24.4 ± 3.9	–	-25.1
Nabberu	PPRG 089	1.85	Top of Frere Fm., Earaheedy Group, Nabberu Basin, Western Australia	25.0 ± 5.5	–	-29.0
Gunflint	3 of 6/30/84	1.88	Schreiber Beach, Gunflint Iron Fm., Ontario, Canada	4.4 ± 2.2	7.3 ± 0.5	-34.5
	PPRG 134			4.1 ± 3.4	–	-33.5
Wabigoon	PPRG 325	2.70	Steep Rock Group, Wabigoon Belt, Western Superior Province, Canada	27.7 ± 3.7	–	-31.3
Farrel Quartzite	MGTKS1	3.02	Mount Grant, Gorge Creek Group, Pilbara Craton, Australia	22.7 ± 3.9	19.8 ± 0.1	-33.2
Josefsdal	99SA07	3.30	Top of Kromberg Fm., Onverwacht Group, Barberton Greenstone Belt, South Africa	21.8 ± 1.1	–	-26.8
Buck Reef	99SA03	3.42	Base of Kromberg Fm., Onverwacht Group, Barberton Greenstone Belt, South Africa	19.5 ± 3.2	15.0 ± 0.4	-24.8

Oxygen Isotope Composition of Water Derived from Kerogens

For most samples the calculated $\delta^{18}O_{water}$ are consistent within errors with a value around 0 ± 2 ‰ (Fig. 2a). Overall, the O isotope composition of water reconstructed from the O isotope composition of kerogens up to *ca.* 3.5 Ga is, therefore, indistinguishable from that of present-day seawater. This is consistent

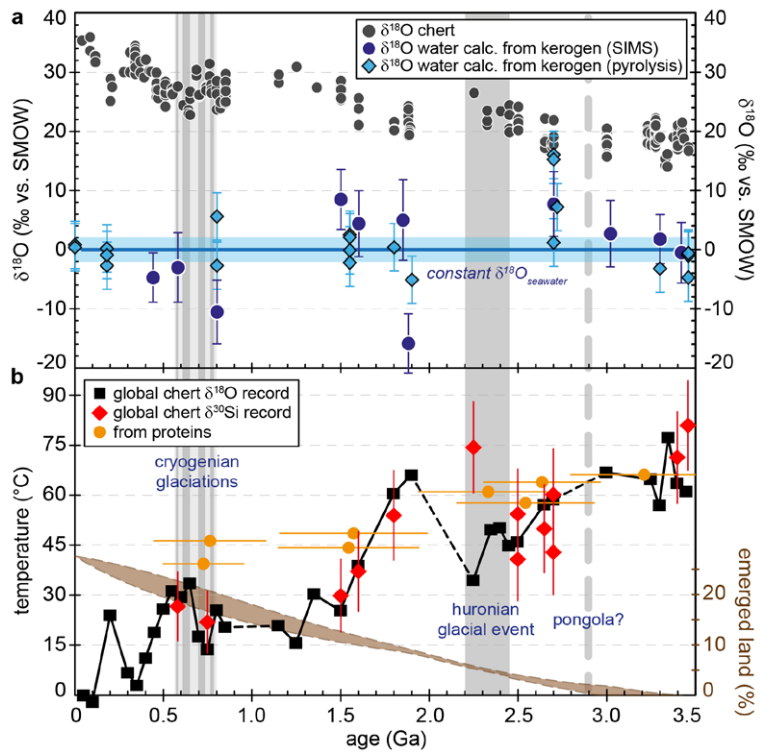

Figure 2 **(a)** Comparison of the chert and calculated seawater O isotope composition evolution through time, calculated using a $\Delta^{18}O_{kerogen\text{-}water}$ of 20 ± 4 ‰. Errors bars correspond to the propagated uncertainties on calculated $\delta^{18}O_{water}$ (including the standard deviation – 1 SD – on average kerogen $\delta^{18}O$ values and the uncertainty of ±4 ‰ on $\Delta^{18}O_{kerogen\text{-}water}$). The horizontal blue band represents a constant $\delta^{18}O_{seawater}$ of 0 ± 2 ‰ through time. **(b)** Estimates of water *T* calculated using (i) the available maximum $\delta^{18}O_{chert}$ value (to which 3 ‰ has been added to take into account possible effects induced by diagenesis – see Supplementary Information) per 50 Ma age intervals and using $\delta^{18}O_{seawater}$ = 0 ± 2 ‰, (ii) the chert $\delta^{30}Si$ record (Robert and Chaussidon, 2006) and (iii) resurrected proteins of ancient bacteria (Gaucher *et al.*, 2008). Estimates of the surface of emerged land through time are also shown (Flament *et al.*, 2013). Vertical grey bars running across both panels correspond to the major glaciation events identified in the geological record (after Hambrey and Harland, 1985, Evans *et al.*, 1997 and Young, 2014).

with inferences made from the study of seawater-altered Precambrian oceanic crust remnants (*e.g.*, Lécuyer and Allemand, 1999; Pope *et al.*, 2012), but does not support a *ca.* 10-15 ‰ progressive increase of $\delta^{18}O_{seawater}$ since 3.5 Ga (Kasting *et al.*, 2006; Jaffrés *et al.*, 2007).

Kerogens from the 1.88 Ga Gunflint Formation collected at Schreiber Beach yielded low $\delta^{18}O$ values of *ca.* 4 ‰, corresponding to a $\delta^{18}O_{water}$ of around -15 ‰ (Fig. 3). A possible interpretation is that this low $\delta^{18}O_{water}$ corresponds to cold shallow waters with a restricted connection with the open ocean and affected by a large influx of low $\delta^{18}O$ continental waters, similar to the present-day Baltic Sea, for example ($\delta^{18}O_{water}$ of -4 to -8 ‰; Jasechko *et al.*, 2013). This hypothesis would imply that the Gunflint cherts formed at low $T < 10$ °C, which is not incompatible with the palaeolatitude of *ca.* 45 °N estimated for that region at 1.88 Ga (see Supplementary Information). On the other hand, kerogens from the 2.7 Ga Belingwe (Manjeri Fm.) and Ventersdorp samples yielded elevated $\delta^{18}O$ values of *ca.* 35 ‰, corresponding to $\delta^{18}O_{water}$ of ~15 ‰ (Fig. 3). A possible interpretation is that precursor OM of these kerogens thrived in warm waters undergoing intense evaporation, which is consistent with the continental depositional environments proposed for these formations (Buck, 1980; Hunter *et al.*, 1998).

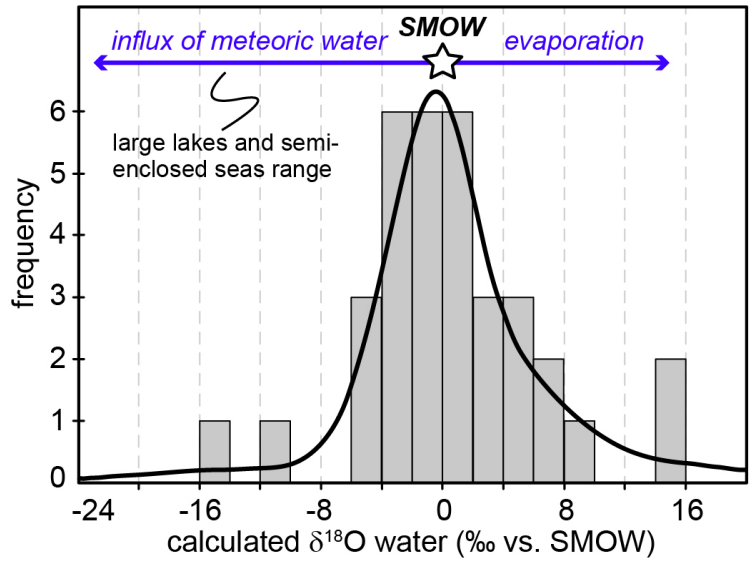

Figure 3 O isotope composition of waters in which precursor biomass of the studied kerogens lived. SMOW corresponds to the present-day mean seawater composition. The range of $\delta^{18}O$ values for large lakes and semi-enclosed seas is after Jasechko *et al.* (2013).

Implications for Surface Temperatures on the Earth during the Precambrian

A globally constant $\delta^{18}O_{seawater}$ around 0 ± 5 ‰ through time, as demonstrated by the present results, implies that Precambrian cherts record formation *T* decreasing from 50-60 °C during the Archean to 0-15 °C for the recent Phanerozoic (Fig. 2b). For some Precambrian formations these elevated precipitation *T* may reflect mixing of seawater with hot hydrothermal fluids (*e.g.*, de Wit and Furnes, 2016). Also, some chert units may have been deposited in environments disconnected from the global oceans. However, taken as a whole the secular decrease of the $\delta^{18}O_{chert}$ record, constructed from 569 individual $\delta^{18}O_{chert}$ analyses representing a worldwide sampling, indicates a global cooling of the conditions on the Earth surface over geological time (Fig. 2b). This is consistent with other estimates such as the temperature of stability measured for resurrected proteins presumably akin those of Precambrian bacteria (Gaucher *et al.*, 2008; Fig. 2b). Elevated *T* around 35-50 °C at 2.2-2.5 Ga appear in conflict with the existence of widespread cold surface conditions during the 'Huronian Glacial Event'. However, there is still no definitive proof supporting a worldwide extent for Huronian glaciations (Young, 2014). Also, global glacial episodes are relatively short (few hundred thousand to a few million years; Prave *et al.*, 2016) so a set of Precambrian chert samples, which are often poorly dated, defining the $\delta^{18}O_{chert}$ for a given 50 Ma time interval, may not have formed contemporaneously with a known glacial period. Finally, it is important to note that reconstructed *T* have remained below *ca.* 30 °C for the past 1.5 Ga, well within the range allowing development of complex eukaryotic life (*e.g.*, Clarke, 2014).

Elevated surface *T* of ~40-60 °C during Archean times, when the Sun was 20-25 % fainter than today (Gough, 1981), required an effective greenhouse atmosphere that may have been controlled by high pressures of CO_2 (P_{CO2}) and of CH_4 (P_{CH4}) (*e.g.*, Kasting and Ono, 2006). Recent 3D Global Climate Model simulations yielded average surface *T* of ~20 °C around 3.4 Ga for P_{CO2} and P_{CH4} of 0.1 bar and 2 mbar, respectively (Charnay *et al.*, 2013). Further simulations also show that higher mean surface *T* (up to *ca.* 50 °C) can be obtained by combining P_{N2} and P_{CO2} of 0.5 bar (Supplementary Information). Such atmospheric pressures are not in contradiction with measurements of $N_2/^{36}Ar$ in Archean hydrothermal fluids (Marty *et al.*, 2013) and studies of fossil imprints of 2.7 Ga rain droplets (Som *et al.*, 2012), which suggest maximum $P_{N2} = 1.1$ bar and $P_{CO2} = 0.7$ bar around 3.0-3.5 Ga (Marty *et al.*, 2013). Finally, the progressive decrease of surface *T* reconstructed from the chert record is inversely correlated with progressive emerging of the continents since *ca.* 3.0 Ga (Fig. 2b). This relationship suggests that the first order control on Earth surface *T* at a geological time scale is the consumption and sequestration of atmospheric CO_2 by weathering of silicates on continental surfaces followed by carbonate deposition (*e.g.*, Berner *et al.*, 1983).

Acknowledgements

This research is supported by the ERC Grant No. 290861 – PaleoNanoLife (PI F. Robert). We thank J.M. Hayes for invaluable discussions, S.M. Awramik, J.W. Schopf, K. Sugitani and F. Westall for providing us with the studied chert samples, and two reviewers for their constructive comments. This is IPGP contribution #3790 and CRPG contribution #2464.

Editor: Bruce Watson

Additional Information

Supplementary Information accompanies this letter at www.geochemicalperspectivesletters.org/article1706

Reprints and permission information is available online at http://www.geochemicalperspectivesletters.org/copyright-and-permissions

Cite this letter as: Tartèse, R., Chaussidon, M., Gurenko, A., Delarue, F., Robert, F. (2017) Warm Archean oceans reconstructed from oxygen isotope composition of early-life remnants. *Geochem. Persp. Let.* 3, 55-65.

References

Berner, R.A., Lasaga, A.C., Garrels, R.M. (1983) The carbonate-silicate geochemical cycle and its effect on atmospheric carbon dioxide over the past 100 million years. *American Journal of Science* 283, 641-683.

Buck, S.G. (1980) Stromatolite and ooid deposits within the fluvial and lacustrine sediments of the Precambrian Ventersdorp Supergroup of South Africa. *Precambrian Research* 12, 311-330.

Charnay, B., Forget, F., Wordsworth, R., Leconte, J., Millour, E., Codron, F., Spiga, A. (2013) Exploring the faint young Sun problem and the possible climates of the Archean Earth with a 3-D GCM. *Journal of Geophysical Research: Atmospheres* 118, 10,414-10,431.

Clarke, A. (2014) The thermal limits to life on Earth. *International Journal of Astrobiology* 13, 141-154.

De Gregorio, B.T., Sharp, T.G., Rushdi, A.I., Simoneit, B.R.T. (2011) Bugs or Gunk? Nanoscale Methods for Assessing the Biogenicity of Ancient Microfossils and Organic Matter. In: Golding, S.D., Glikson, M. (Eds.) *Earliest Life on Earth: Habitats, Environments and Methods of Detection.* Springer, Netherlands, 239-289.

Delarue, F., Rouzaud, J.-N., Derenne, S., Bourbin, M., Westall, F., Kremer, B., Sugitani, K., Deldicque, D., Robert, F. (2016) The Raman-derived carbonization continuum: A tool to select the best preserved molecular structures in Archean kerogens. *Astrobiology* 16, 407-417.

de Wit, M.J., Furnes, H. (2016) 3.5-Ga hydrothermal fields and diamictites in the Barberton Greenstone Belt – Paleoarchean crust in cold environments. *Science Advances* 2, e1500368.

Evans, D.A., Beukes, N.J., Kirschvink, J.L. (1997) Low-latitude glaciation in the Palaeoproterozoic era. *Nature* 386, 262-266.

Flament, N., Coltice, N., Rey, P. (2013) The evolution of the $^{87}Sr/^{86}Sr$ of marine carbonates does not constrain continental growth. *Precambrian Research* 229, 177-188.

Gaucher, E.A., Govindarajan, S., Ganesh, O.K. (2008) Palaeotemperature trend for Precambrian life inferred from resurrected proteins. *Nature* 451, 704-707.

Gough, D.O. (1981) Solar interior structure and luminosity variations. *Solar Physics* 74, 21-34.

Hambrey, M.J., Harland, W.B. (1985) The Late Proterozoic glacial era. *Palaeogeography, Palaeoclimatology, Palaeoecology* 51, 255-272.

Hunter, M.A., Bickle, M.J., Nisbet, E.G., Martin, A., Chapman, H.J. (1998) Continental extensional setting for the Archean Belingwe Greenstone Belt, Zimbabwe. *Geology* 26, 883-886.

Jaffrés, J.B.D., Shields, G.A., Wallmann, K. (2007) The oxygen isotope evolution of seawater: A critical review of a long-standing controversy and an improved geological water cycle model for the past 3.4 billion years. *Earth-Science Reviews* 83, 83-122.

Jasechko S., Sharp, Z.D., Gibson, J.J. Birks, S.J., Yi, Y., Fawcett, P.J. (2013) Terrestrial water fluxes dominated by transpiration. *Nature* 496, 347-351.

Kasting, J.F., Ono, S. (2006) Palaeoclimates: the first two billion years. *Philosophical Transactions of the Royal Society B* 361, 917-929.

Kasting, J.F., Tazewell Howard, M., Wallmann, K., Veizer, J., Shields, G., Jaffrés, J. (2006) Paleoclimates, ocean depth, and the oxygen isotopic composition of seawater. *Earth and Planetary Science Letters* 252, 82-93.

Knauth, L.P., Epstein, S. (1976) Hydrogen and oxygen isotope ratios in nodular and bedded cherts. *Geochimica et Cosmochimica Acta* 40, 1095-1108.

Knauth, L.P., Lowe, D.R. (2003) High Archean climatic temperature inferred from oxygen isotope geochemistry of cherts in the 3.5 Ga Swaziland Supergroup, South Africa. *Geological Society of America Bulletin* 115, 566-580.

Lécuyer, C., Allemand, P. (1999) Modelling of the oxygen isotope evolution of seawater: Implications for the climate interpretation of the $\delta^{18}O$ of marine sediments. *Geochimica et Cosmochimica Acta* 63, 351-361.

Marin-Carbonne, J., Chaussidon, M., Robert, F. (2012) Micrometer-scale chemical and isotopic criteria (O and Si) on the origin and history of Precambrian cherts: implications for paleotemperature reconstructions. *Geochimica et Cosmochimica Acta* 92, 129-147.

Marty, B., Zimmermann, L., Pujol, M., Burgess, R., Philippot, P. (2013) Nitrogen isotopic composition and density of the Archean atmosphere. *Science* 342, 101-104.

Pope, E.C., Bird, D.K., Rosing, M.T. (2012) Isotope composition and volume of Earth's early oceans. *Proceedings of the National Academy of Science of the United States of America* 109, 4371-4376.

Prave, A.R., Condon, D.J., Hoffmann, K.H., Tapster, S., Fallick, A.E. (2016) Duration and nature of the end-Cryogenian (Marinoan) glaciation. *Geology* 44, 631-634.

Robert, F., Chaussidon, M. (2006) A palaeo-temperature curve for the Precambrian oceans based on silicon isotopes in cherts. *Nature* 443, 969-972.

Roden, J.S., Ehleringer, J.R. (2000) There is no temperature dependence of net biochemical fractionation of Hydrogen and Oxygen isotopes in tree-ring cellulose. *Isotopes in Environmental and Health Studies* 36, 303-317.

Schmidt, H.L., Robins, R.J., Werner, R.A. (2015) Multi-factorial in vivo stable isotope fractionation: causes, correlations, consequences and applications. *Isotopes in Environmental and Health Studies* 51, 155-199.

Som, S.M., Catling, D.C., Harnmeijer, J.P., Polivka, P.M., Buick, R. (2012) Air density 2.7 billion years ago limited to less than twice modern levels by fossil raindrop imprints. *Nature* 484, 359-362.

Sternberg, L., Ellsworth, P.F.V. (2011) Divergent biochemical fractionation, not convergent temperature, explains cellulose Oxygen isotope enrichment across latitudes. *PLoS ONE* 6, e28040.

Tartèse, R., Chaussidon, M., Gurenko, A., Delarue, F., Robert, F. (2016) *In situ* oxygen isotope analysis of fossil organic matter. *Geochimica et Cosmochimica Acta* 182, 24-39.

Wedeking, K.W. (1983) The Biogeochemistry of Precambrian Kerogen. Ph.D. thesis, Indiana University, 167 pp.

Williford, K.H., Ushikubo, T., Schopf, J.W., Lepot, K., Kitajima, K., Valley, J.W. (2013) Preservation and detection of microstructural and taxonomic correlations in the carbon isotopic compositions of individual Precambrian microfossils. *Geochimica et Cosmochimica Acta* 104, 165-182.

Young, G.M. (2014) Contradictory correlations of Paleoproterozoic glacial deposits: Local, regional or global controls? *Precambrian Research* 247, 33-44.

Warm Archean oceans reconstructed from oxygen isotope composition of early-life remnants

R. Tartèse[*1,2], M. Chaussidon[3], A. Gurenko[4], F. Delarue[1], F. Robert[1]

Supplementary Information

The Supplementary Information includes:

- Studied samples
- Methods
- Compositions of the studied kerogens
- Oxygen isotope fractionation between organic matter and water
- Oxygen isotopes in cherts
- Climate modelling for the early Earth
- Figures S-1 to S-4
- Tables S-1 to S-5
- Supplementary Information References

Studied Samples

Doushantuo. The Doushantuo chert sample 1a of 8/25/83, sampled by S.M. Awramik, comes from the Yangtze Gorges, South China (Awramik *et al.*, 1985). The Doushantuo Formation comprises dark dolomite with chert interbedded with

1. Institut de Minéralogie, de Physique des Matériaux et de Cosmochimie (IMPMC), Sorbonne Universités, UPMC Univ Paris 06, MNHN, CNRS, IRD, 75005 Paris, France
2. Department of Physical Sciences, The Open University, Walton Hall, MK7 6AA Milton Keynes, United Kingdom
* Corresponding author (email: romain.tartese@mnhn.fr)
3. Institut de Physique du Globe de Paris (IPGP), Université Sorbonne-Paris-Cité, CNRS UMR 7154, 75238 Paris Cedex 05, France
4. Centre de Recherches Pétrographiques et Géochimiques, UMR 7358, Université de Lorraine, 54501 Vandoeuvre-lès-Nancy, France

shale. It is famous for the occurrence of well-preserved, abundant and diverse microfossils forming benthic mat biota (bacteria, cyanobacteria) and planktonic remnants that thrived in the overlying water column. The age of the Doushantuo microfossils is not precisely known. The Doushantuo Formation itself has been dated between *ca*. 635 Ma and 550-555 Ma (Condon *et al*., 2005; Zhang *et al*., 2005) and we have attributed here an age of ~575 Ma for the studied chert sample.

Bitter Springs. The Bitter Springs chert sample 3 of 11/2/90, sampled by S.M. Awramik, comes from the Ross River Area in the Bitter Springs Formation, Amadeus Basin, Northern Territory, Australia, and is known to contain colonial and filamentous cyanobacteria microfossils (Barghoorn and Schopf, 1965; Schopf, 1968). As summarised by Schopf (1968), the Bitter Springs Formation is predominantly composed of dark grey laminated cherty limestone and dolomite, interbedded with thin units of siltstone and dark shale. Evaporitic deposits (gypsum, halite) are locally abundant at the bottom of the Bitter Springs Formation, while algal stromatolites, commonly associated with dark chert lenses and nodules, are particularly developed in its middle and upper portions. The Bitter Springs Formation, whose age is relatively well constrained at *ca*. 800 Ma, has been subdivided into the lower Gillen Member and upper Loves Creek Member, the latter being further subdivided into three units, the uppermost of which containing the studied microfossil assemblages (Barghoorn and Schopf, 1965; Schopf, 1968). The depositional environment of the microfossil-bearing units of the Bitter Springs Formation is debated. Initially, Schopf (1968) described the Bitter Springs Formation deposition as starting with sand to silt deposition in a gradually subsiding basin in which evaporites precipitated in restricted, disconnected, areas, followed by the widespread development of algae in a shallow sea environment. Based notably on C and S isotope evidence, recent studies have argued that the microfossil-bearing upper unit of the Loves Creek Member was deposited in a non-marine environment such as a hypersaline lake (Hill and Walter, 2000; Hill *et al*., 2000), an interpretation refuted by Lindsay *et al*. (2005) who favoured a shallow marine tidal environment.

Jixian. The Jixian chert sample 1 of 8/14/83, sampled by S.M. Awramik, comes from the Mesoproterozoic Gaoyuzhuang Group, which constitutes one of the four groups comprising the *ca*. 10 km thick Proterozoic sedimentary succession outcropping near the city of Jixian on the northern margin of the North China Block (Lu *et al*., 2008). At the type section the Gaoyuzhuang Group is ~1600 m thick and subdivided into 4 formations that mostly consist of varied dolostone units, stromatolite assemblages and chert layers frequently hosting carbonaceous microfossils (*e.g.*, Zhang, 1981; Schopf *et al*., 1984; Xu and Awramick, 2002). A few Pb-Pb dates obtained on galena from Pb-Zn SEDEX mineralised horizons belonging to the Gaoyuzhuang Group yielded dates ranging between *ca*. 1350 and 1485 Ma (Cheng *et al*., 1981), suggesting that the depositional age of the group may be close to 1500 Ma. Recently, U-Pb dating on zircon from a tuff bed in the Gaoyuzhuang Group yielded an age of 1560 Ma (Li *et al*., 2010). Overall, the voluminous carbonate succession of the Gaoyuzhuang Group was deposited between 1.4 and 1.6 Ga.

McArthur. The McArthur chert sample 7 of 6/21/90, sampled by S.M. Awramik, comes from the Palaeoproterozoic to Mesoproterozoic McArthur Basin, Northern Territory, Australia. The McArthur basin is a ~5-15 km thick sequence of mostly unmetamorphosed sedimentary and associated volcanic rocks deposited on the North Australian Craton between around 1.8 and 1.4 Ga (Rawlings, 1999). It comprises a mixture of carbonate and siliciclastic successions, with minor volcanic units near the base (Rawlings, 1999). Several microfossil-rich occurrences have been described in stromatolitic chert horizons throughout the McArthur basin (*e.g.*, Muir, 1976; Oehler, 1978).

Gunflint. Kerogens were isolated from two Gunflint chert samples, sample 3 of 6/30/84, sampled by S.M. Awramik, and sample PPRG 134 (Walter *et al*., 1983). Both samples were collected from the lower chert horizon of the Gunflint Iron Formation, *ca*. 5 km west of the Schreiber beach locality, on the northern shore of the Lake Superior (Ontario, Canada). Cherts at this locality are famous for their abundance of well-preserved microfossils (Barghoorn and Tyler, 1965; Cloud, 1965; Awramik and Barghoorn, 1977; Alleon *et al*., 2016), indicative of the pristine nature of the Gunflint Formation there, and of the fact that it experienced conditions only slightly above burial diagenesis (Winter and Knauth, 1992; Marin *et al*., 2010). The Gunflint Iron Formation, dated at *ca*. 1.88 Ga (Fralick *et al*., 2002), which is part of the Animikie basin, was deposited in shallow waters in a subsiding basin with a restricted connection with the open ocean (Carrigan and Cameron, 1991; Schulz and Cannon, 2007), at a palaeolatitude of around 45 °N (Pesonen *et al*., 2012).

Nabberu. The Nabberu chert sample PPRG 089 was collected from beds transitional between the Frere and Windidda Formations in the Lake Carnegie area, Earaheedy Basin, Western Australia (Walter *et al*., 1983). Recent sedimentological and stratigraphic studies carried out in the Earaheedy Basin, synthesised in Pirajno *et al.* (2009), indicate that the Windidda Member is in fact part of the top of the Frere Formation. The Frere Formation overlies the Yelma Formation, which constitutes the base of the Earaheedy Group, and was deposited *ca*. 1.89 Ga (Rasmussen *et al*., 2012) on the Yilgarn continental margin during a marine transgression, in a shallow water environment as indicated by the presence of varied types of stromatolites (Pirajno *et al*., 2009; Akin *et al*., 2013). The *ca*. 500 m thick Frere Formation is unmetamorphosed and consists of alternating beds of chloritic siltstone, haematitic shale and granular iron formation, the latter horizons being typically 0.5-20 cm thick and containing granular iron beds intercalated with shale, siltstone, jasper and chert (Pirajno *et al*., 2009). These granular iron formations of the Frere Formation are comparable to those of the Lake Superior region in Canada, and host microfossil assemblages similar to those described in the contemporaneous Gunflint Iron Formation (Walter *et al*., 1976; Tobin, 1990).

Wabigoon. The Wabigoon chert sample PPRG 325 was collected at the South Robert Pit locality (48.798333 °N; 91.639722 °W), in the Steep Rock Group, Wabigoon Belt, Western Superior Province, Canada (Walter *et al*., 1983). The Steep Rock Group overlies the 3.0 Ga tonalitic gneiss of the Marmion Complex and

comprises three units, from base to top, the detrital Wagita Formation (sandstone and conglomerate), the stromatolite-bearing Mosher Carbonate and the iron-rich Jolliffe Ore Zone (*e.g.*, Wilks and Nisbet, 1988; Fralick and Riding, 2015). Units of the Steep Rock Group were regionally metamorphosed in the lower greenschist facies (Wilks and Nisbet, 1985). Detailed sedimentological, petrological and geochemical studies of the ~500 m thick Mosher Carbonate show that it is essentially composed by limestone that accumulated on a shallow marine platform environment on the 3.0 Ga eroded crystalline basement during a marine transgression, precipitating from oxygenated seawater according to REE geochemistry (Fralick and Riding, 2015 and references therein). Therefore, the *ca*. 2.7-2.8 Ga Steep Rock stromatolites may have hosted oxygenic photosynthetic cyanobacteria and could constitute an early example of a marine oxygen oasis (Fralick and Riding, 2015).

Farrel Quartzite. The chert sample MGTKS1 was collected by K. Sugitani in a black chert horizon from the *ca*. 3.0 Ga Farrel Quartzite in the Mount Grant area, part of the Mount Goldsworthy greenstone belt in the northeastern Pilbara Craton, Australia (Sugitani *et al.*, 2007). This greenstone belt comprises a lower unit composed essentially of volcanic sequences older than 3.17 Ga and an upper sedimentary succession, the 3.02-2.93 Ga De Grey Supergroup (Van Kranendonk *et al*., 2007). The lower part of the De Grey Supergroup is known as the 3.02 Ga Gorge Creek Group, which comprises a clastic formation (the Farrel Quartzite), and an upper formation of chert, banded iron formation, black shale, and siltstone (the Cleaverville Formation). The Farrel Quartzite is up to 80 m thick and contains fine- to very coarse-grained sandstone, minor conglomerate units, mafic to ultra-mafic volcanoclastic layers, evaporite beds and black chert layers (Sugitani *et al*., 2007). These units were metamorphosed to lower greenschist facies and pervasively silicified. The *ca*. 30 cm thick microfossil-bearing black chert occurs in the uppermost part of the Farrel Quartzite and is closely associated with evaporite beds. This black chert-evaporite association can be traced for *ca*. 7 km along strike in the central and the western parts of the greenstone belt. Morphologically diverse carbonaceous microstructures have been identified from the black cherts (Sugitani *et al*., 2007), whose biogenic origin has been determined through multidisciplinary studies (Grey and Sugitani, 2009; Oehler *et al*., 2009; Sugitani *et al*., 2009; House *et al.*, 2013).

Josefsdal. The Josefsdal chert sample 99SA07, collected by F. Westall, was sampled from a chert horizon at the top of the Kromberg Formation in the Onverwacht Group in the upper part of the Josefsdal Valley (25.959490 °S; 31.073787 °E), near the village of Msauli in the Barberton Greenstone Belt, South Africa (Westall *et al*., 2006). This chert horizon consists of two chert layers separated by silicified pillow basalt, and sample 99SA07 was collected from the upper layer. The black and white/green banded chert horizons consist of silicified volcanoclastic sediments displaying sedimentary structures indicative of deposition in a shallow water environment. These units have been subjected to low-grade metamorphism (lowermost greenschist facies). Combined morphological and chemical characteristics of carbonaceous microstructures suggest that they represent the fossilised

remains of photosynthesising microbial mats that thrived in a nearshore volcanogenic sedimentary setting, and whose development was strongly influenced by contemporaneous hydrothermal fluids (Westall *et al*., 2011, 2015).

Buck Reef. The Buck Reef Chert sample 99SA03, collected by F. Westall, was sampled at the base of the Kromberg Formation, Onverwacht Group, in the Barberton Greenstone Belt (South Africa) (Westall *et al*., 2001). The Buck Reef Chert is *ca*. 3.42 Ga old, 250-400 m-thick, and has been metamorphosed to lower greenschist facies. Petrological and geochemical studies indicate that the Buck Reef Chert was deposited under gradually increasing water depths in environments that ranged from shallow coastal lagoons to an open marine platform, with limited influence of local hydrothermal systems and detrital input (Tice, 2009; Tice and Love, 2004, 2006). It has been proposed that carbonaceous matter in the Buck Reef Chert originated from photosynthetic mats developed in the euphotic zone, later dispersed as detrital carbonaceous matter by waves and currents (Tice, 2009; Tice and Love, 2004, 2006).

Carbon isotope compositions of the studied samples. The C isotope compositions given in Table 1 are from Guo *et al*. (2006) for Doushantuo (average of $\delta^{13}C_{org}$ values obtained on 12 chert samples); Beaumont and Robert (1999) for Bitter Springs, Wabigoon and Gunflint 3 of 6/30/84 samples; Hayes *et al.* (1983) for McArthur (average of $\delta^{13}C$ values obtained on samples 103-1, 106-1, 107-1 and 452-1) and Nabberu (PPRG 089) samples; Strauss and Moore (1992) for Jixian (average of $\delta^{13}C$ values obtained on PPRG samples 1422, 1432, 2125 and 2126 from the Gaoyuzhuang Fm.) and Gunflint PPRG 134 (labelled PPRG 1289 in their Table 17.1) samples; Sugahara *et al.* (2010) for the Farell Quartzite sample MGTKS1 (average of $\delta^{13}C$ values obtained on samples labelled CE2 in their Table 1); Westall *et al.* (2006) for Josefsdal and Hren *et al.* (2009) for Buck Reef (average of $\delta^{13}C$ values obtained on chert samples with $\delta^{18}O > 18$ ‰).

Methods

Kerogen analysis. Kerogens were isolated from the host chert samples through successive demineralisations using an HF-HCl acidic treatment (Durand and Nicaise, 1980), and then ground into a fine powder, from which ~10 mg was used for bulk kerogen O isotope analysis and a few mg were pressed into high purity indium and then carbon coated for secondary electron microscopy (SEM) and SIMS investigations.

Bulk kerogen O isotope compositions were determined by thermal conversion elemental analysis – isotope ratio mass spectrometry (TC/EA-IRMS) at Iso-Analytical Ltd. (Cheshire, UK) following the protocol reported in Tartèse *et al*. (2016).

O isotope compositions of the kerogen samples were also measured using the Cameca IMS 1280 HR and IMS 1270 E7 ion probe instruments at the Centre de Recherches Pétrographiques et Géochimiques (CRPG) in Nancy (France)

during several analytical sessions and using identical analytical protocols to those described in detail in Tartèse *et al.* (2016). Isotopes of ^{16}O and ^{18}O were first analysed using a Cs^+ primary beam of ~10 nA with an acceleration voltage of 10 kV rastered over 10 × 10 µm diameter areas. Negative secondary ions were accelerated at 10 kV and measured in multicollection mode using two Faraday cups (FC) on the L'2 trolley for ^{16}O and on the H1 trolley for ^{18}O and a mass resolving power of ~2500 (using slit #1 in multicollection mode). For each analysis, the FC backgrounds were measured during pre-sputtering, and the measured $^{18}O/^{16}O$ ratios were corrected for FC background using the average of background measurements performed immediately before (during pre-sputtering of analysis *n*) and immediately after (during pre-sputtering of analysis *n+1*). The total analytical time for O isotope analysis was ~5-6 min, including pre-sputtering (60 s) and counting the secondary oxygen ions during 50-60 cycles each of 5 s.

The secondary species $^{12}C^1H$, ^{16}O, ^{28}Si, ^{32}S and $^{56}Fe^{16}O$ were then collected during separate acquisition using the magnetic peak switching mode on the same analytical spots using a ~1-10 nA Cs^+ beam, depending on C and O intensities, in order to identify and filter the data affected by contamination of organic matter (OM) by residual silica minerals, sulphides, Fe-chromite or Fe-oxides (see details in Tartèse *et al.*, 2016). All the measured oxygen isotope compositions and secondary species intensity are reported in Table S-4.

The final uncertainties for individual $\delta^{18}O$ values, reported in Table S-5 at the 2σ level, include uncertainties related to counting statistics associated with each individual analysis and the external reproducibility measured on the Clarno kerogen standard ($\delta^{18}O_{bulk}$ = 14.3 ± 0.1 ‰; Tartèse *et al.*, 2016), which was also used to correct the measured $\delta^{18}O$ values for instrumental mass fractionation.

O isotope analysis in chert samples by SIMS. O isotope compositions of three black bedded chert samples from the 3.0 Ga Farrel Quartzite Formation (samples CRT, GTEV and GW98) were measured using the CAMECA IMS 1280 HR ion probe at the Centre de Recherches Pétrographiques et Géochimiques (CRPG) in Nancy (France) following the analytical protocol described in Marin *et al.* (2010). The final uncertainties reported for $\delta^{18}O$ values, reported in Table S-3 at the 1σ level, include uncertainties related to counting statistics associated with each individual analysis and the external reproducibility measured on the quartz and Miocene chert internal standards, which were also used to correct the measured $\delta^{18}O$ values for instrumental mass fractionation.

Compositions of the Studied Kerogens

Bulk O isotope compositions. Thermal combustion EA-IRMS analyses on four selected kerogen samples ranging in age from 0.58 Ga to 3.42 Ga yielded bulk O abundances between 7.0 and 26.1 wt. %, a range similar to the one reported for Phanerozoic coal and kerogen samples (Tartèse *et al.*, 2016). The associated bulk kerogen $\delta^{18}O$ values range between 7.3 ± 1.0 ‰ and 19.8 ± 0.1 ‰ (Table 1).

SIMS elemental contents and O isotopes. Large variations of $^{12}C^1H$, ^{16}O, ^{28}Si, ^{32}S and $^{56}Fe^{16}O$ intensities are observed at the ~20-30 µm spot scale in each sample (Fig. S-2), which is similar to the results obtained on Phanerozoic coal and kerogen samples (Tartèse *et al.*, 2016). For each sample, the relationships between measured ^{16}O, ^{28}Si, ^{32}S and $^{56}Fe^{16}O$ *vs.* $^{12}C^1H$ intensities generally trend towards the diagram origin in Figure S-2, caused by the variable secondary ion emission for each analysis due to topography and surface flatness effects (resulting from the fact that OM powders were pressed into indium). It is thus not possible to convert these measured intensities directly into C (or O, Si, S, *etc.*) abundances. However, these intensities are typical of those measured on coal and kerogen samples, ranging, for example, between ~3 × 10^6 and ~2-3 × 10^7 cps nA^{-1} for $^{12}C^1H$ intensities (Fig. S-2), which roughly correspond to bulk C contents of around 30 to 75 wt. % (Tartèse *et al.*, 2016). For ^{16}O, most analyses range between ~5 × 10^6 and 10^8 cps nA^{-1} (Fig. S-2), corresponding to O contents of ~7-8 to 25 wt. % (Tartèse *et al.*, 2016), which are typical for kerogens (Durand and Monin, 1980). The O abundance measured in Josefsdal is slightly higher than this range. Intensities of ^{32}S mostly fall in the range ~10^6-10^8 cps nA^{-1} (Fig. S-2), indicating bulk organic S contents around 0.5-2.5 wt. % (Tartèse *et al.*, 2016). The kerogens display a large range of ^{28}Si intensities, between ~10^3 and 3-4 × 10^6 cps nA^{-1} (Fig. S-2). The lower end of this range, up to ~10^5 cps nA^{-1}, is similar to the ^{28}Si intensities obtained on Phanerozoic coals and kerogens (Tartèse *et al.*, 2016). Finally, $^{56}Fe^{16}O$ intensities on the studied kerogens range between ~10^3 and 2-3 × 10^5 cps nA^{-1} and are similar to those obtained on Phanerozoic coals and kerogens (Tartèse *et al.*, 2016).

The procedure we employed to filter the SIMS analyses contaminated by sputtering of micro-inclusions of mineral phases is described in detail in Tartèse *et al.* (2016) and only summarised here. In pure, homogeneous, organic matter the effect of sample surface topography should theoretically result in mixing trends pointing to the origin in binary diagrams (where ^{16}O, ^{28}Si, ^{32}S and $^{56}Fe^{16}O$ signals are plotted against the $^{12}C^1H$ intensity) because of variations in emissivity. We interpret outliers to such trends as reflecting the presence of mineral inclusions in the corresponding sputtered volume. In binary diagrams of ^{16}O, ^{28}Si, ^{32}S and $^{56}Fe^{16}O$ *versus* $^{12}C^1H$, we calculated linear regressions passing through the origin for each sample, together with their 5σ confidence intervals, which ensures that only true outliers are discarded and not analyses resulting from the local chemical variability of OM. We then excluded outliers falling outside these 5σ confidence intervals as they likely correspond to analyses contaminated by the presence of micro-mineral inclusions. We developed this statistical approach to avoid the ambiguity of 'visually' filtering out data.

The studied kerogens display several per mille variations in their oxygen isotopic composition at the micrometre scale (Fig. S-1). For each sample, individual $\delta^{18}O$ values display unimodal Gaussian distributions around the mean value (Fig. S-1), indicating that there is no evidence for multiple O-bearing organic components with varied O isotope compositions in the kerogens. The good consistency between thermal combustion EA-IRMS and SIMS average $\delta^{18}O$

values obtained on selected samples (Table 1) indicates that most of the SIMS $\delta^{18}O$ variability at the sample scale can be assigned to the combined contribution of several analytical effects, such as:

- **Topography:** even though kerogen samples have been pressed into indium so that their surface is flat, this creates porosity between organic matter grains, which may result in a few per mille uncertainty in measured $\delta^{18}O$ values.
- **Instrumental Mass Fractionation (IMF):** measured $\delta^{18}O$ values have been corrected for IMF using analyses carried out on the Clarno kerogen standard (Tartèse *et al.*, 2016). Since there is currently only one kerogen O isotope SIMS standard, it is not possible to assess the possible effects of variable H/C and O/C ratios on IMF of O isotopes. It has been shown that variable H/C ratios induce a few per mille variations of IMF for C isotope analysis by SIMS for example (Sangély *et al.*, 2005). Furthermore, it is likely that H/C and O/C ratios are slightly variable from spot-to-spot in each sample. Altogether this may add a few per mille intra-sample $\delta^{18}O$ variability.
- **Sputtering micro-mineral inclusions:** measurements of the $^{12}C^{1}H$, ^{16}O, ^{28}Si, ^{32}S and $^{56}Fe^{16}O$ intensities for each SIMS spot in which O isotopes were measured allow us to filter out the data compromised by sputtering micro-mineral inclusions (Tartèse *et al.*, 2016). However, this process would not filter out compromised data when micro-mineral inclusions have been completely sputtered away during the O isotope analysis that we carried out before analysis of $^{12}C^{1}H$, ^{16}O, ^{28}Si, ^{32}S and $^{56}Fe^{16}O$.
- **Low ^{18}O count rates:** due to the low abundance of O in some of the studied kerogen samples, the ^{18}O intensities measured using a Faraday cup were often low. We have shown previously that measurements with these low ^{18}O count rates (typically between 10^5 to 10^6 cps) yielded accurate $\delta^{18}O$ average values (see Fig. 1 in Tartèse *et al.*, 2016). However, low ^{18}O count rates increase the dispersion of $\delta^{18}O$ values around the mean, which may, therefore, increase the $\delta^{18}O$ variability measured at the sample scale.

For all samples the range and average $\delta^{18}O$ values obtained by SIMS on the studied kerogens are listed in the Table S-2.

Oxygen Isotope Fractionation between Organic Matter and Water

As stated in the main text, metabolic exchanges with their environment largely determined the isotopic composition of biomolecules synthesised by living organisms. In aquatic organisms *ca.* 70-80 % of OM oxygen is derived from the water in which they thrive and the remainder from their diet (Kreuzer-Martin and Jarman, 2007; Wang *et al.*, 2009; Soto *et al.*, 2013; Mayr *et al.*, 2015). However,

during thermal maturation of OM, chemical and structural changes occur, such as aromatisation due to the loss of hydrogenated and oxygenated groups, which may then alter the original organic O isotope compositions.

O-rich components (*e.g.*, carbohydrates, amino acids) are quickly degraded during early OM maturation, resulting in the formation of insoluble kerogens dominated by thermally-resistant components (*e.g.*, aromatic moieties). Investigating this potential issue, Zech *et al.* (2012) showed that neither fractionation nor exchange reactions affected the O isotope composition of carbohydrates during cellulose decomposition over a 27 month period. On the other hand, litter decomposition was accompanied by a diminution of the bulk OM $\delta^{18}O$ values, reflecting changes in the relative proportions of O-bearing compounds having different O isotope compositions. Similarly, experiments simulating diagenetic alteration of algal biomass at 80 °C and pH 1-2 have shown that ~70 % of O bound to biomolecules during hydrolytic solubilisation of algal biomass does not exchange with water (Wedeking and Hayes, 1983).

Proto-kerogen samples derived from marine algae collected in surface sediments from the Atlantic and Pacific oceans, and isolated from Lower Jurassic Toarcian shales are characterised by consistent $\delta^{18}O$ values of 20.4 ± 1.5 ‰, 20.8 ± 1.1 ‰ and 18.9 ± 1.5 ‰ (Wedeking, 1983). Taking $\delta^{18}O_{seawater}$ values of 0 ‰ for the present-day ocean (in which the precursor biomass of the proto-kerogen samples thrived) and -1 ‰ for the Toarcian ocean (an ice-free ocean in which the precursor biomass of the Toarcian proto-kerogens lived), we can calculate a $\Delta^{18}O_{organics\text{-}water}$ ($\delta^{18}O_{organics} - \delta^{18}O_{water}$) of 20.4 ± 0.9 ‰ (2 SD). Such a $\Delta^{18}O_{kerogen\text{-}water}$ is consistent with the value we estimated for the O isotope fractionation between fossilised cyanobacteria and waters from the lakes Magadi-Natron in East Africa in which their precursor biomass lived (Tartèse *et al.*, 2016). Altogether, these data indicate that the O isotope composition of proto-kerogen is similar to that of O bound to carboxyl functional groups, which does not seem to be fractionated during OM maturation.

Oxygen Isotopes in Cherts

Chert-based oxygen isotope thermometry. The O isotope composition of chert ($\delta^{18}O_{chert}$) is related to the O isotope composition of the fluid ($\delta^{18}O_{water}$) from which it precipitated, and the temperature T at which precipitation occurred, and follows the empirical equation derived by Knauth and Epstein (1976):

$$1000 \ln\alpha_{chert\text{-}water} = 3.09 \times 10^6/T^2 - 3.29$$
$$\approx \Delta^{18}O_{chert\text{-}water} = (\delta^{18}O_{chert} - \delta^{18}O_{water}) \qquad \text{Eq. S-1}$$

Therefore, interpreting the chert O isotope record in terms of precipitation T, or the O isotope composition of surface water (ocean or lake) from which chert precipitated, implies the assumption of one of these two parameters. As a result, two end-member scenarios can explain the ~10-15 ‰ increase of $\delta^{18}O$ values

measured in cherts from *ca*. 3.5 Ga to the present-day: (i) cherts precipitated at low *T* from waters that were characterised by $\delta^{18}O$ values ~10-15 ‰ lower compared to today (Perry, 1967; Kasting *et al*., 2006; Jaffrés *et al*., 2007; Hren *et al*., 2009), or (ii) cherts precipitated at *T* ~50-70 °C higher than today from waters with O isotope compositions comparable to those of present-day surface waters (Knauth and Epstein, 1976; Knauth and Lowe, 1978, 2003; Robert and Chaussidon, 2006). For Precambrian cherts, there are additional uncertainties regarding the type of waters from which they precipitated (*e.g.*, open marine, restricted lakes, evaporative brine, pore water), and the possibility of post-crystallisation exchange of oxygen isotopes with meteoric or formation water during diagenesis.

Microscale heterogeneity of $\delta^{18}O_{chert}$ and implications for temperature reconstructions. The detailed SIMS study carried out by Marin *et al*. (2010) on five Gunflint chert samples allowed them to identify large and randomly distributed $\delta^{18}O$ variations (up to ~14 ‰ at the 2 µm scale) in microquartz, showing that it preserved O isotope heterogeneity acquired during its formation through diagenesis. Considering that microquartz formed by a dissolution/precipitation process from amorphous silica precipitated at equilibrium with seawater, Marin *et al*. (2010) were able to reproduce the average and the distribution of $\delta^{18}O$ values measured in Gunflint cherts. Their results suggest that cherts precipitated at 37 to 52 °C from water with a $\delta^{18}O$ of -1 ‰ and continued to exchange with 30 % pore water during diagenesis at temperatures of 130 to 170 °C. One of the major outcomes of this study is that temperatures calculated from bulk and average SIMS $\delta^{18}O$ values measured on chert samples may be *ca*. 15-20 °C too high, since diagenesis results in bulk $\delta^{18}O_{chert}$ values a few per mille lower than those of amorphous silica precursors. The difference is about 3 ‰ for the Gunflint chert samples studied by Marin *et al*. (2010).

To test whether similar effects also apply to older samples we carried out SIMS analyses at a ~20 µm scale in three chert samples from the Farrel Quartzite Formation (see description of the studied samples above). These three samples yielded very similar results, with average $\delta^{18}O$ values of 16.4-17.3 ‰ and ranges of $\delta^{18}O$ values of 5.5-6.5 ‰ at the ~20 µm scale (Table S-3). Such ranges are consistent with those measured at the 20 µm scale on Gunflint chert samples, indicating that 'true' (*i.e.* calculated at the 2 µm scale) $\delta^{18}O$ ranges for the Farrel Quartzite chert samples are probably around ~12.5 to 13.5 ‰ (Table S-3). The average and the range of $\delta^{18}O$ values of Farrel Quartzite chert samples can be reproduced for temperatures of precipitation of around 80 °C (from water with a $\delta^{18}O$ of 0 ‰) and diagenetic temperatures around 250 °C (still considering 30 % pore water) (Fig. S-4a), which corresponds to the lower greenschist conditions experienced by the Farrel Quartzite Formation (Sugitani *et al*., 2007). Similarly to the observations made for the 1.9 Ga Gunflint samples, this simple modelling shows that the amorphous silica precursor of the Farrel Quartzite chert samples was characterised by $\delta^{18}O$ values ~3 ‰ higher than the measured bulk/average $\delta^{18}O$ values.

Our SIMS results obtained in Gunflint OM suggest that Gunflint does not represent an open marine environment but may rather correspond to a mid- to high-latitude basin with restricted connection to the open ocean, in which silica crystallised from low $\delta^{18}O$ water. Therefore, considering that this silica formed from water with a $\delta^{18}O$ of -10 ‰ and contained 30 % pore water with the same O isotope composition, calculations using the model of Marin *et al*. (2010) yield a bulk chert $\delta^{18}O$ value of 22.2 ‰ and a larger range for $\delta^{18}O$ variations of 20.7 ‰, for T_{water} and $T_{diagenesis}$ of 5 °C and 130 °C, respectively (Fig. S-4b).

Considering the observations detailed above, we propose a new palaeotemperature evolution curve ranging from 3.5 Ga to the present-day, recalculated from the chert O isotope record by considering the maximum $\delta^{18}O_{chert}$ values per 50 Ma bin intervals (using $\delta^{18}O_{chert}$ data from Knauth, 2005; Knauth and Epstein, 1976; Knauth and Lowe, 1978, 2003; Robert and Chaussidon, 2006; and this study), and adding 3 ‰ to these maximum $\delta^{18}O$ values, since it is likely that $\delta^{18}O$ values in most, if not all, chert samples were affected to a similar extent by diagenetic dissolution/precipitation processes. As a result, our new $\delta^{18}O_{chert}$-derived palaeotemperature curve (see Fig. 2 in the main text) is shifted by 10-20 °C compared to those calculated in previous studies.

Climate Modelling for the Early Earth

Using recent 3D Global Climate Model simulations, Charnay *et al*. (2013) have argued that atmospheric CO_2 and CH_4 partial pressures of 0.1 bar and 2 mbar, respectively, could have sustained an average surface *T* of ~20 °C around 3.4 Ga. Further simulations have also shown that even higher mean surface *T* of *ca*. 50 °C can be obtained combining P_{N2} = 0.5 bar and P_{CO2} = 0.5 bar (for P_{CH4} between 0 and 1 mbar), and up to *ca*. 70 °C combining P_{N2} = 1 bar and P_{CO2} = 1 bar (for P_{CH4} between 0 and 2 mbar) (Charnay, 2014). If elevated atmospheric pressures of 1 bar for N_2 and CO_2 may appear too high, those around 0.5 bar fit well with geological observations (see main text).

Supplementary Figures

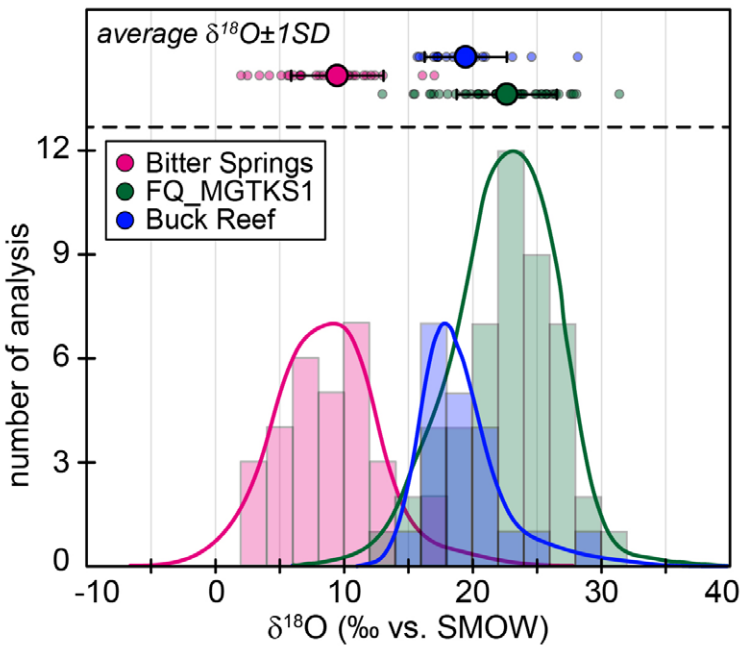

Figure S-1 Distribution of the SIMS $\delta^{18}O$ values measured on three selected kerogen samples. To construct histograms the data have been binned into 2‰ intervals. All individual analyses are displayed by small circles in the upper part of the panel. Large circles and associated error bars correspond to average $\delta^{18}O$ values together with their standard deviation (1 SD).

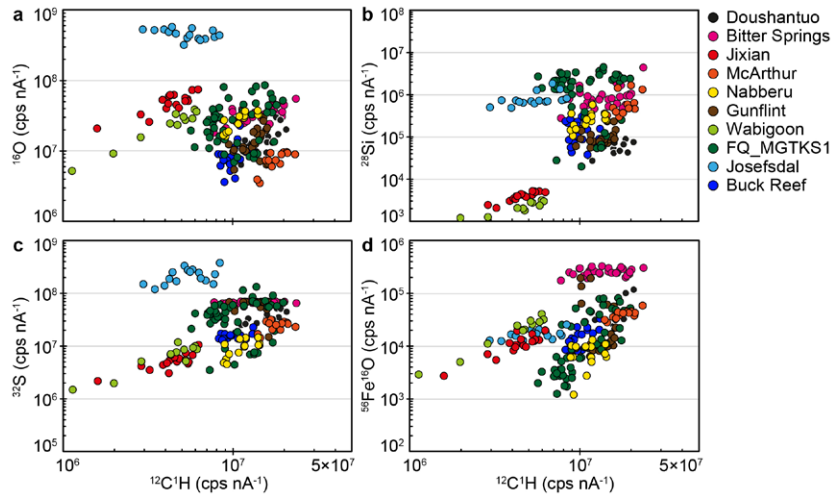

Figure S-2 Measured ^{16}O **(a)**, ^{28}Si **(b)**, ^{32}S **(c)** and $^{56}Fe^{16}O$ **(d)** secondary intensities (normalised to the primary beam intensity) versus $^{12}C^{1}H$ secondary intensity. For each sample, the relationships between measured ^{16}O, ^{28}Si, ^{32}S and $^{56}Fe^{16}O$ vs. $^{12}C^{1}H$ intensities generally trend towards the diagram origin, resulting from variable secondary ion emission for each analysis due to topography and surface flatness effects.

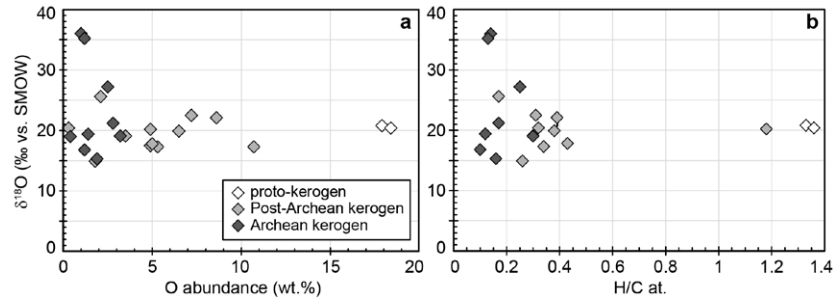

Figure S-3 Oxygen isotope compositions measured in kerogens plotted against their O abundances **(a)** and their H/C atomic ratios **(b)**. The data are from Wedeking (1983).

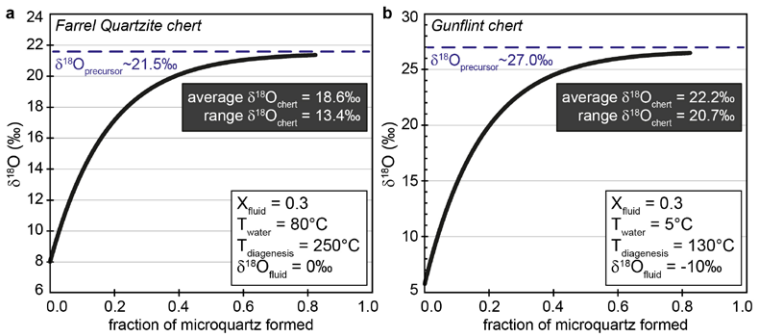

Figure S-4 Evolution of the O isotope composition of microquartz formed from the progressive dissolution of amorphous silica precursors. In **(a)** the parameters used for the calculation, aimed at modelling the SIMS results obtained on the Farrel Quartzite sample CRT, are; 30 % fluid in the initial porosity of the amorphous silica precursors (X_{fluid}), temperatures of 80 °C and 250 °C for the water from which it initially precipitated and for metamorphism, respectively, and a $\delta^{18}O_{water}$ value of 0‰. In **(b)** the parameters used for the calculation, aimed at modelling the SIMS results obtained on Gunflint chert samples, are; X_{fluid} = 30 %, temperatures of 5 °C and 130 °C for the water from which it initially precipitated and for diagenesis/metamorphism, respectively, and a $\delta^{18}O_{water}$ value of -10‰ (see text for details).

Supplementary Tables

Table S-1 Bulk H/C, O contents and O and C isotope compositions obtained by pyrolysis on chert-extracted kerogen samples by Wedeking (1983). $\delta^{13}C$ and the $\delta^{18}O$ values are given relative to VPDB and SMOW, respectively. All the samples, except recent sediments and Lower Toarcian shales, are PPRG samples, whose descriptions are given in Walter *et al.* (1983).

Geological unit	Age (Ga)	Sample	H/C at.	$\delta^{13}C$ (‰)	O (wt. %)	$\delta^{18}O$ (‰)
Sediment, Tanner Basin, Pacific	–		1.33	-21.4	17.9	20.8
Sediment, Walvis Bay, Atlantic	–		1.36	-20.0	18.4	20.4
Lower Toarcian shales, Paris Basin, France	0.18	10968	1.32	-28.0	10.7	17.3
	0.18	11933	1.18		4.9	20.2
	0.18	15035	1.05		3.5	19.1
Skillogallee, Adelaide Geosyncline, Australia	0.80	455-1	0.17	-23.2	2.1	25.6
Bitter Springs Fm., Amadeus basin, Australia	0.80	133-2	0.34	-22.4	5.3	17.3
	0.80	133-2			4.9	17.5
Bungle Bungle Fm., Birrindudu basin, Australia	1.55	159-1	0.31	-30.0	7.2	22.5
	1.55	138-1	0.38	-30.2	6.5	19.9
	1.55	154-1	0.39	-30.7	8.6	22.1
	1.55	152-1	0.43	-29.3	5.0	17.8
Duck Creek dolomite, Wyloo Gr., Ashburton Trough, Australia	1.80	060-1	0.32	-31.7	0.3	20.4
McLeary Fm., Belcher Gr., Ontario, Canada	1.90	447-1	0.26	-28.4	1.8	14.9
Ventersdorp Fm. Ventersdorp, South Africa	2.70	293-1	0.14	-38.5	1.0	36.0
Steeprock Lake Fm., Wabigoon Belt, Ontario, Canada	2.70	325-1	0.17	-27.2	2.8	21.2
Manjeri Fm., Belingwe Greenstone Belt, Zimbabwe, Africa	2.70	225-1	0.13	-33.2	1.2	35.2
Tumbiana Fm., Fortescue Gr., Hamersley Basin, Australia	2.72	027-1	0.25	-51.2	2.5	27.2
Szwartkoppie Fm., Barberton Greenstone Belt, South Africa	3.30	198-1	0.10	-32.0	1.2	16.8
Towers Fm., Warrawoona Gr., Pilbara Block, Australia	3.46	002-1	0.30	-34.3	3.2	19.1
	3.46	004-1	0.16	-36.0	1.9	15.3
Warrawoona Gr., Pilbara Block, Australia	3.46	016-1	0.30	-35.2	0.4	19.0
Hooggenoeg Fm., Barberton Greenstone Belt, South Africa	3.46	182-1	0.12	-31.6	1.4	19.4

Table S-2 O isotope characteristics of the kerogens analysed by SIMS.

Sample	Reference	Analyses	SIMS $\delta^{18}O$ values (‰)			
			Min.	Max.	Average	1 SD
Doushantuo	1a of 8/25/83	13	9.2	24.7	17.0	4.3
Bitter Springs	3 of 11/2/90	30	2.0	17.0	8.6	3.7
Jixian	1 of 8/14/83	17	21.7	33.1	28.5	3.1
McArthur	7 of 6/21/90	13	16.7	29.6	24.4	3.9
Nabberu	PPRG 089	14	16.1	33.3	25.0	5.5
Gunflint	3 of 6/30/84 & PPRG 134	24	-2.5	10.6	4.2	3.0
Wabigoon	PPRG 325	11	19.4	33.3	27.7	3.7
Farrel Quartzite	MGTKS1	49	13.2	31.6	22.7	3.9
Josefsdal	99SA07	16	19.6	23.9	21.8	1.1
Buck Reef	99SA03	20	15.9	28.4	19.5	3.2

Table S-3 Oxygen isotope results obtained by SIMS on the Farrel Quartzite chert samples. The 2 µm range has been calculated from the range of $\delta^{18}O$ values measured at the 20 µm scale and the relationship between analysis scale and $\delta^{18}O$ range of Marin *et al.* (2010).

Analysis	$\delta^{18}O$ (‰)	1σ (‰)	Analysis	$\delta^{18}O$ (‰)	1σ (‰)	Analysis	$\delta^{18}O$ (‰)	1σ (‰)
CRT 1	14.4	0.5	GTEV 1	17.2	0.2	GW98-1-48 A	18.9	1.0
CRT 5	17.3	0.9	GTEV 2	16.9	0.3	GW98-1-48 B	20.4	1.0
CRT 6	14.2	0.7	GTEV 3 A	17.4	0.3	GW98-1-50	16.8	0.5
CRT 8	18.1	0.7	GTEV 3 B	17.3	0.4	GW98-1-51	14.2	1.0
CRT 9	17.1	0.6	GTEV 4	18.5	1.1	GW98-1-53	15.1	1.1
CRT 10	17.6	0.6	GTEV 4-2	15.3	0.3	GW98-1-54	18.7	1.1
CRT 11	18.8	0.5	GTEV 6-1 A	15.2	0.2	GW98-1-55	15.9	0.7
CRT 12	18.8	0.7	GTEV 6-1 B	15.7	0.7	GW98-1-56	13.9	1.2
CRT 13	20.5	0.6	GTEV 6-2	15.8	0.3	GW98-1-57	14.6	0.7
CRT 14	19.9	0.6	GTEV 8	19.5	0.6	GW98-1-58	14.8	0.4
CRT 15	16.2	0.6	GTEV 10	17.2	1.2	GW98-1-59	18.6	0.3
CRT 17	15.1	0.3	GTEV 13-1	14.3	0.9	GW98-1-62	14.2	0.5
CRT 18 A	18.1	1.1	GTEV 13-2	14.5	0.4	GW98-1-63	16.6	0.3
CRT 18 B	17.8	0.8	GTEV 15	14.0	0.6	GW98-1-99	18.0	1.1
CRT 19	14.6	0.6	GTEV 18-1	15.5	0.8			
CRT 21	17.6	1.4	GTEV18-2	16.0	0.4			
CRT 22	14.6	0.8	GTEV 21-5	18.0	0.4			
CRT 23	19.9	1.2	GTEV 30	15.4	0.4			
CRT 24	17.9	0.3	GTEV 32	17.4	0.8			
Average	17.3		**Average**	16.4		**Average**	16.5	
1 SD	2.0		**1 SD**	1.5		**1 SD**	2.1	
Max.	20.5		**Max.**	19.5		**Max.**	20.4	
Min.	14.2		**Min.**	14.0		**Min.**	13.9	
Range	6.3		**Range**	5.5		**Range**	6.5	
2 µm range	13.4		**2 µm range**	12.5		**2 µm range**	13.6	

Table S-4 All oxygen isotope and chemistry data collected by SIMS. Analyses in purple are those that have been filtered, and grey boxes indicate based on which element between O, Si, S and Fe (see text for details).

Sample	Analysis Name	X	Y	^{16}O (cps/nA)	^{18}O (cps/nA)	meas. $\delta^{18}O$ (‰)	1σ (‰)	mass 12.8 (cps)	^{12}CH (cps/nA)	^{16}O (cps/nA)	^{28}Si (cps/nA)	^{32}S (cps/nA)	^{56}FeO (cps/nA)
Doushantuo	Doushantuo@1	8751	-920	2.10E+07	3.42E+04	-13.64	0.62	-9.33E+04	1.86E+07	1.74E+07	9.03E+04	3.55E+07	9.86E+04
1a of 8/25/83	Doushantuo@02	8631	-929	1.72E+07	2.65E+04	-5.34	0.51	-9.38E+04	1.58E+07	1.90E+07	5.32E+04	3.60E+07	2.36E+04
	Doushantuo@03	8537	-938	2.60E+07	4.43E+04	-8.46	0.64	-9.39E+04	1.62E+07	1.60E+07	9.08E+04	3.55E+07	3.04E+04
	Doushantuo@04	8595	-991	1.14E+07	1.43E+04	-15.51	1.05	-9.59E+04	1.12E+07	6.40E+06	3.53E+04	2.54E+07	8.66E+03
	Doushantuo@05	8658	-1185	1.80E+07	2.79E+04	-10.38	0.81	-9.57E+04	1.59E+07	1.34E+07	7.27E+04	3.15E+07	2.09E+04
	Doushantuo@06	8849	-1195	1.91E+07	3.01E+04	-8.72	0.58	-9.47E+04	1.38E+07	9.96E+06	5.96E+04	2.74E+07	1.19E+04
	Doushantuo@07	9022	-1203	4.19E+07	7.58E+04	-16.10	0.33	-9.67E+04	1.58E+07	9.53E+06	4.22E+04	4.01E+07	1.44E+04
	Doushantuo@08	9134	-1296	2.79E+07	4.78E+04	-9.99	0.36	-8.96E+04	1.81E+07	3.01E+07	6.72E+04	5.22E+07	3.19E+04
	Doushantuo@09	8968	-1328	5.42E+07	1.01E+05	-15.52	0.26	-8.86E+04	1.91E+07	2.76E+07	4.32E+04	5.17E+07	4.85E+04
	Doushantuo@10	8767	-1346	2.23E+07	3.66E+04	-12.75	0.53	-9.32E+04	2.07E+07	2.02E+07	7.65E+04	4.50E+07	1.15E+05
	Doushantuo@11	8568	-1355	4.00E+07	7.17E+04	-20.83	0.25	-9.41E+04	1.23E+07	1.30E+07	5.51E+04	3.35E+07	3.07E+04
	Doushantuo@12	8473	-1445	3.45E+07	6.11E+04	-14.99	0.37	-9.30E+04	1.71E+07	1.32E+07	4.73E+04	3.27E+07	2.04E+04
	Doushantuo@15	8620	-1637	1.60E+07	2.35E+04	-16.99	0.35	-9.42E+04	1.18E+07	1.42E+07	2.76E+04	2.65E+07	1.54E+04
	Doushantuo@16	8414	-1550	4.30E+07	7.82E+04	-14.34	0.27	-9.02E+04	1.93E+07	2.86E+07	1.96E+05	4.66E+07	3.81E+04
	Doushantuo@17	8279	-1639	4.80E+07	8.80E+04	-17.24	0.23	-8.82E+04	1.57E+07	3.08E+07	3.31E+04	5.34E+07	3.15E+04
Bitter Springs	Bitter@02	794	-554	4.69E+07	8.54E+04	-23.50	0.34	-7.62E+04	1.47E+07	2.97E+07	7.87E+05	6.47E+07	2.52E+05
3 of 11/2/90	Bitter@03	754	-554	7.01E+07	1.32E+05	-20.70	0.24	-7.48E+04	7.54E+06	4.70E+07	1.39E+06	6.97E+07	3.87E+05
	Bitter@05	674	-554	7.09E+07	1.34E+05	-19.38	0.62	-7.51E+04	1.31E+07	3.03E+07	8.29E+05	6.63E+07	2.30E+05
	Bitter@07	594	-554	8.48E+07	1.63E+05	-13.01	0.52	-7.59E+04	1.14E+07	3.94E+07	7.80E+05	6.70E+07	2.61E+05
	Bitter@08	554	-554	4.87E+07	8.93E+04	-18.36	0.23	-7.22E+04	1.72E+07	4.98E+07	9.09E+05	6.64E+07	2.77E+05
	Bitter@09	514	-554	4.48E+07	8.07E+04	-26.44	0.36	-7.62E+04	6.47E+06	2.68E+07	3.74E+05	6.65E+07	3.04E+05
	Bitter@10	514	-514	4.16E+07	7.46E+04	-24.50	0.30	-8.06E+04	7.73E+06	1.83E+07	2.81E+05	6.84E+07	1.71E+05
	Bitter@11	554	-514	3.92E+07	6.98E+04	-23.44	0.35	-7.25E+04	1.05E+07	4.32E+07	7.82E+05	6.78E+07	3.87E+05
	Bitter@12	594	-514	4.26E+07	7.62E+04	-27.55	0.30	-7.39E+04	1.35E+07	3.51E+07	1.03E+06	6.78E+07	3.18E+05
	Bitter@13	634	-514	4.67E+07	8.42E+04	-28.04	0.37	-7.74E+04	1.17E+07	2.50E+07	7.85E+05	6.57E+07	2.71E+05
	Bitter@14	674	-514	1.06E+08	2.05E+05	-13.50	0.19	-6.52E+04	8.53E+06	6.67E+07	2.29E+06	6.90E+07	4.05E+05
	Bitter@15	714	-514	4.01E+07	7.17E+04	-21.98	0.35	-7.48E+04	1.95E+07	3.09E+07	1.03E+06	6.57E+07	2.27E+05
	Bitter@16	754	-514	3.61E+07	6.39E+04	-19.12	0.37	-7.60E+04	1.11E+07	2.96E+07	5.83E+05	6.74E+07	2.24E+05
	Bitter@17	794	-514	2.87E+07	4.85E+04	-26.61	0.30	-7.80E+04	1.47E+07	3.21E+07	5.34E+05	6.60E+07	2.94E+05
	Bitter@18	834	-514	4.37E+07	7.91E+04	-20.01	0.37	-7.60E+04	1.10E+07	2.84E+07	6.60E+05	6.72E+07	1.89E+05

Sample	Analysis Name	X	Y	^{16}O (cps/nA)	^{18}O (cps/nA)	meas. $\delta^{18}O$ (‰)	1σ (‰)	mass 12.8 (cps)	^{12}CH (cps/nA)	^{16}O (cps/nA)	^{28}Si (cps/nA)	^{32}S (cps/nA)	^{56}FeO (cps/nA)
	Bitter@19	834	-474	4.41E+07	8.02E+04	-17.65	0.26	-7.35E+04	2.01E+07	4.50E+07	1.08E+06	7.01E+07	2.75E+05
	Bitter@20	794	-474	6.93E+07	1.30E+05	-26.63	0.31	-7.08E+04	9.17E+06	5.40E+07	1.39E+06	7.02E+07	3.52E+05
	Bitter@21	754	-474	4.49E+07	8.15E+04	-20.20	0.42	-7.80E+04	1.22E+07	2.66E+07	4.70E+05	7.01E+07	2.55E+05
	Bitter@22	714	-474	3.84E+07	6.82E+04	-22.26	0.41	-7.51E+04	8.66E+06	2.82E+07	8.03E+05	6.55E+07	2.44E+05
	Bitter@23	674	-474	6.65E+07	1.26E+05	-13.96	0.18	-7.43E+04	1.54E+07	3.35E+07	8.31E+05	6.84E+07	2.38E+05
	Bitter@24	634	-474	4.00E+07	7.15E+04	-24.37	0.54	-7.39E+04	1.05E+07	2.59E+07	5.28E+05	6.37E+07	2.08E+05
	Bitter@25	594	-474	3.12E+07	5.41E+04	-18.53	0.46	-7.62E+04	1.86E+07	3.36E+07	5.83E+05	6.35E+07	1.96E+05
	Bitter@26	554	-474	4.85E+07	8.86E+04	-20.80	0.21	-7.51E+04	1.89E+07	3.15E+07	9.59E+05	6.72E+07	2.10E+05
	Bitter@27	514	-474	3.53E+07	6.20E+04	-29.11	0.45	-7.81E+04	6.25E+06	1.97E+07	3.08E+05	6.58E+07	2.56E+05
	Bitter@29	554	-434	4.65E+07	8.48E+04	-18.77	0.29	-7.29E+04	2.81E+07	4.43E+07	1.29E+06	6.76E+07	2.17E+05
	Bitter@30	594	-434	3.06E+07	5.24E+04	-23.50	0.37	-7.69E+04	1.65E+07	2.42E+07	6.23E+05	6.80E+07	2.37E+05
	Bitter@31	634	-434	5.60E+07	1.03E+05	-26.35	0.28	-7.29E+04	7.65E+06	6.10E+07	4.00E+05	6.55E+07	6.28E+05
	Bitter@32	674	-434	7.18E+07	1.36E+05	-17.03	0.34	-7.40E+04	9.93E+06	3.96E+07	1.68E+06	6.57E+07	2.87E+05
	Bitter@33	714	-434	3.49E+07	6.11E+04	-25.82	0.50	-7.33E+04	1.63E+07	4.19E+07	1.99E+06	6.96E+07	2.36E+05
	Bitter@34	754	-434	2.95E+07	5.02E+04	-24.92	0.39	-7.65E+04	9.12E+06	2.11E+07	2.34E+05	6.63E+07	2.26E+05
	Bitter@35	794	-434	6.60E+07	1.24E+05	-19.67	0.25	-6.99E+04	2.36E+07	5.53E+07	4.46E+06	6.58E+07	2.96E+05
	Bitter@36	834	-434	3.82E+07	6.79E+04	-22.50	0.60	-7.60E+04	3.26E+06	2.94E+07	2.49E+05	6.58E+07	2.74E+05
	Bitter@37	834	-394	4.01E+07	7.18E+04	-21.29	0.37	-7.51E+04	1.79E+07	3.47E+07	4.88E+05	7.07E+07	2.85E+05
	Bitter@38	794	-394	4.65E+07	8.48E+04	-18.00	0.40	-7.55E+04	1.30E+07	3.28E+07	7.71E+05	6.66E+07	2.38E+05
	Bitter@39	754	-394	5.90E+07	1.09E+05	-27.74	0.30	-7.53E+04	5.80E+06	2.67E+07	2.47E+05	6.91E+07	2.95E+05
	Bitter@40	714	-394	9.39E+07	1.80E+05	-17.01	0.17	-6.88E+04	1.08E+07	5.58E+07	3.76E+06	6.75E+07	2.86E+05
	Bitter@41	674	-394	4.90E+07	8.96E+04	-21.12	0.28	-6.53E+04	1.50E+07	7.06E+07	2.42E+07	7.37E+07	8.10E+05
	Bitter@42	634	-394	5.20E+07	9.53E+04	-23.96	0.45	-7.07E+04	1.74E+07	3.84E+07	1.70E+06	6.78E+07	3.05E+05
	Bitter@43	594	-394	3.82E+07	6.77E+04	-23.37	0.57	-7.56E+04	1.18E+07	3.47E+07	6.33E+05	7.06E+07	3.13E+05
	Bitter@44	554	-394	4.77E+07	8.70E+04	-21.61	0.34	-7.47E+04	1.96E+07	3.60E+07	9.55E+05	6.63E+07	2.45E+05
	Bitter@45	514	-394	3.79E+07	6.72E+04	-22.50	0.38	-7.77E+04	2.26E+06	2.79E+07	4.79E+05	6.74E+07	2.58E+05
	Bitter@46	474	-394	1.86E+07	2.83E+04	-31.67	0.74	-7.83E+04	5.71E+06	1.89E+07	1.99E+05	7.26E+07	1.99E+05
	Bitter@47	434	-394	8.01E+07	1.52E+05	-23.48	0.31	-7.08E+04	1.00E+07	3.60E+07	1.11E+06	6.79E+07	2.91E+05
	Bitter@49	354	-394	4.50E+07	8.14E+04	-23.53	0.25	-7.23E+04	9.19E+06	4.29E+07	1.08E+06	6.69E+07	2.82E+05
	Bitter@50	314	-394	4.33E+07	7.81E+04	-19.80	0.44	-7.63E+04	1.11E+07	2.90E+07	9.34E+05	7.09E+07	2.31E+05
Jixian	Jixian@1	-4218	-23	8.39E+07	1.88E+05	-1.70	0.20	3.80E+04	7.46E+06	6.22E+07	1.25E+04	5.87E+07	6.76E+04
1 of 8/14/83	Jixian@02	-4178	-23	9.62E+07	2.12E+05	-0.52	0.38	3.74E+04	5.08E+06	6.31E+07	1.19E+04	1.10E+07	2.93E+04

Sample	Analysis Name	X	Y	^{16}O (cps/nA)	^{18}O (cps/nA)	meas. $\delta^{18}O$ (‰)	1σ (‰)	mass 12.8 (cps)	^{12}CH (cps/nA)	^{16}O (cps/nA)	^{28}Si (cps/nA)	^{32}S (cps/nA)	^{56}FeO (cps/nA)
	Jixian@03	-4138	-23	8.03E+07	1.80E+05	-3.34	0.34	3.89E+04	1.34E+06	2.51E+07	8.28E+03	1.39E+06	1.30E+04
	Jixian@04	-4098	-23	1.32E+08	2.83E+05	-6.51	0.22	3.74E+04	1.83E+06	7.99E+07	9.80E+03	3.94E+06	4.05E+04
	Jixian@05	-4058	-23	8.17E+07	1.82E+05	-11.37	0.32	3.67E+04	3.22E+06	2.60E+07	9.44E+03	3.57E+06	1.28E+04
	Jixian@06	-4018	-23	5.49E+07	1.30E+05	-4.06	0.41	3.70E+04	9.65E+05	1.97E+07	8.43E+03	1.20E+06	1.13E+04
	Jixian@07	-3978	-23	1.24E+08	2.67E+05	-2.19	0.21	3.75E+04	4.68E+06	7.20E+07	1.18E+04	4.48E+06	2.32E+04
	Jixian@08	-3938	-23	7.49E+07	1.69E+05	-10.96	0.37	3.70E+04	1.59E+06	2.07E+07	8.41E+03	2.13E+06	1.06E+04
	Jixian@09	-3898	-23	1.37E+08	2.93E+05	-2.11	0.14	3.92E+04	5.42E+06	5.52E+07	1.27E+04	4.81E+06	2.04E+04
	Jixian@10	-3858	-23	7.52E+07	1.70E+05	-4.30	0.30	3.82E+04	4.22E+06	6.02E+07	1.22E+04	5.37E+06	1.86E+04
	Jixian@11	-3858	17	5.26E+07	1.26E+05	-1.88	0.42	3.75E+04	3.81E+06	2.96E+07	1.06E+04	8.00E+06	1.70E+04
	Jixian@12	-3898	17	8.63E+06	3.88E+04	-12.38	2.27	3.75E+04	1.54E+05	1.73E+06	7.61E+03	1.98E+05	9.05E+03
	Jixian@13	-3938	17	6.30E+07	1.46E+05	-7.09	0.30	3.69E+04	2.87E+06	3.28E+07	9.94E+03	4.14E+06	1.43E+04
	Jixian@14	-3978	17	4.42E+07	1.08E+05	-15.01	0.42	3.55E+04	5.84E+06	2.20E+07	1.09E+04	3.00E+06	1.15E+04
	Jixian@15	-4018	17	4.93E+07	1.19E+05	-10.53	0.43	3.68E+04	1.75E+06	2.18E+07	9.15E+03	1.83E+06	1.26E+04
	Jixian@16	-4058	17	8.06E+07	1.81E+05	-7.02	0.31	4.08E+04	6.19E+06	4.00E+07	1.19E+04	9.28E+06	2.81E+04
	Jixian@17	-4098	17	2.70E+07	7.49E+04	-6.96	0.69	3.83E+04	3.02E+05	6.76E+06	7.88E+03	6.59E+06	1.13E+04
	Jixian@18	-4138	17	6.62E+07	1.52E+05	-5.97	0.36	3.86E+04	3.37E+05	1.89E+07	8.27E+03	5.01E+05	1.24E+04
	Jixian@19	-4178	17	7.51E+07	1.70E+05	-4.19	0.25	3.84E+04	5.24E+06	5.68E+07	1.18E+04	7.53E+06	2.44E+04
	Jixian@20	-4218	17	1.03E+08	2.26E+05	-0.60	0.47	3.77E+04	3.86E+06	5.34E+07	1.12E+04	4.53E+06	1.97E+04
	Jixian@21	-4218	57	8.71E+07	1.94E+05	-2.61	0.32	3.77E+04	4.66E+06	4.52E+07	1.21E+04	5.11E+06	1.80E+04
	Jixian@22	-4178	57	1.40E+08	3.00E+05	0.11	0.23	3.72E+04	5.77E+06	7.34E+07	1.34E+04	7.03E+06	2.14E+04
	Jixian@23	-4138	57	7.58E+07	1.72E+05	-4.57	0.24	3.80E+04	4.82E+06	4.09E+07	1.15E+04	5.83E+06	1.72E+04
	Jixian@24	-4098	57	1.02E+08	2.25E+05	-0.89	0.18	3.80E+04	2.81E+06	4.59E+07	1.04E+04	5.22E+06	1.95E+04
	Jixian@25	-4058	57	1.06E+08	2.31E+05	-5.19	0.24	3.82E+04	4.00E+06	6.63E+07	1.25E+04	1.24E+07	3.65E+04
	Jixian@26	-4018	57	7.50E+07	1.69E+05	-4.83	0.34	3.75E+04	4.07E+06	4.04E+07	1.15E+04	4.93E+06	1.64E+04
	Jixian@27	-3978	57	8.74E+07	1.94E+05	-3.05	0.21	3.75E+04	5.47E+06	5.13E+07	1.29E+04	5.05E+06	2.11E+04
	Jixian@28	-3938	57	9.31E+07	2.06E+05	-4.33	0.20	3.90E+04	4.51E+06	6.28E+07	1.28E+04	6.30E+06	2.18E+04
	Jixian@29	-3898	57	7.45E+07	1.69E+05	-6.00	0.30	3.89E+04	1.50E+06	3.25E+07	9.36E+03	1.92E+06	1.39E+04
	Jixian@30	-3858	57	4.15E+07	1.03E+05	-13.00	0.46	3.83E+04	9.02E+05	1.70E+07	9.12E+03	1.46E+06	1.18E+04
	Jixian@31	-3858	97	2.93E+07	7.92E+04	-8.63	0.71	3.84E+04	7.19E+05	1.07E+07	8.88E+03	1.09E+06	1.03E+04
	Jixian@32	-3898	97	1.19E+08	2.55E+05	-6.11	0.14	3.63E+04	5.25E+06	5.12E+07	1.25E+04	5.60E+06	1.98E+04
	Jixian@33	-3938	97	8.38E+07	1.87E+05	-4.75	0.18	3.58E+04	4.18E+06	4.72E+07	1.10E+04	3.10E+06	1.71E+04
	Jixian@34	-4018	97	1.00E+08	2.20E+05	-1.65	0.19	3.72E+04	4.28E+06	6.27E+07	1.17E+04	6.91E+06	2.70E+04

Sample	Analysis Name	X	Y	^{16}O (cps/nA)	^{18}O (cps/nA)	meas. $\delta^{18}O$ (‰)	1σ (‰)
	Jixian@35	-4058	97	1.36E+08	2.89E+05	-5.27	0.16
McArthur	McArthur@1	-5594	656	1.43E+08	2.92E+05	-5.96	0.08
7 of 6/21/90	McArthur@02	-5734	671	4.25E+07	9.30E+04	-10.37	0.29
	McArthur@03	-5597	665	1.16E+08	2.39E+05	-3.91	0.09
	McArthur@04	-5602	792	7.32E+07	1.54E+05	-8.96	0.23
	McArthur@05	-5612	867	1.02E+08	2.10E+05	-7.25	0.21
	McArthur@08	-5372	793	1.58E+08	3.22E+05	-3.60	0.29
	McArthur@09	-5389	701	5.47E+07	1.17E+05	-8.78	0.22
	McArthur@10	-5427	642	5.13E+07	1.11E+05	-3.72	0.49
	McArthur@11	-5591	654	8.59E+07	1.79E+05	-5.02	0.12
	McArthur@12	-6509	1757	5.76E+07	1.24E+05	-5.79	0.20
	McArthur@13	-5805	1742	4.76E+07	1.03E+05	-16.35	0.26
	McArthur@14	-5814	1815	5.99E+07	1.27E+05	-13.60	0.33
	McArthur@15	-5881	1861	3.48E+07	7.87E+04	-5.90	0.26
	McArthur@16	-5858	1920	6.16E+07	1.31E+05	-12.55	0.17
	McArthur@18	-5822	2028	6.71E+07	1.43E+05	-1.07	0.19
	McArthur@19	-5838	2086	7.03E+07	1.48E+05	-9.66	0.15
	McArthur@20	-5803	2173	2.82E+07	6.60E+04	0.09	0.38
	McArthur@21	-5844	2232	5.41E+07	1.16E+05	-11.56	0.26
	McArthur@23	-5589	2600	3.94E+07	8.73E+04	-10.08	0.22
	McArthur@24	-5509	2634	7.01E+07	1.49E+05	-3.44	0.25
	McArthur@25	-5414	2637	4.37E+07	9.53E+04	-14.80	0.32
Gunflint	Gunflint@126	-134	3998	1.09E+07	2.13E+04	-26.77	0.67
3 of 6/30/84	Gunflint@127	-84	3998	1.16E+07	2.26E+04	-27.55	0.49
	Gunflint@128	-34	3998	1.96E+07	3.82E+04	-27.15	0.37
	Gunflint@129	16	3998	1.83E+07	3.59E+04	-22.13	0.38
	Gunflint@130	66	3998	1.01E+07	1.99E+04	-27.52	0.86
	Gunflint@131	116	3998	9.68E+06	1.91E+04	-27.42	0.66
	Gunflint@133	216	3998	5.75E+06	1.16E+04	-28.69	1.21
	Gunflint@134	266	3998	1.07E+07	2.10E+04	-28.61	0.49
Gunflint	PPRG134@01	616	-6533	2.50E+07	4.09E+04	-30.35	0.74
PPRG 134	PPRG134@02	656	-6533	4.33E+07	7.70E+04	-33.98	0.24

mass 12.8 (cps)	^{12}CH (cps/nA)	^{16}O (cps/nA)	^{28}Si (cps/nA)	^{32}S (cps/nA)	^{56}FeO (cps/nA)
3.84E+04	6.26E+06	7.53E+07	1.28E+04	1.08E+07	2.78E+04
4.32E+04	2.33E+07	6.04E+07	3.50E+06	6.04E+07	1.53E+05
5.15E+04	2.00E+07	4.12E+07	3.50E+06	5.98E+07	9.60E+04
4.51E+04	1.90E+07	5.50E+07	1.74E+06	5.98E+07	1.32E+05
5.30E+04	1.70E+07	4.82E+07	8.73E+05	5.93E+07	1.13E+05
5.53E+04	1.45E+07	5.93E+07	1.35E+06	5.93E+07	1.18E+05
4.73E+04	1.62E+07	5.93E+07	1.37E+06	5.93E+07	1.51E+05
6.65E+04	2.09E+07	4.49E+07	1.40E+06	5.98E+07	8.58E+04
4.89E+04	1.14E+07	2.87E+07	1.10E+06	5.98E+07	5.25E+04
4.99E+04	1.20E+07	4.36E+07	1.67E+06	5.98E+07	8.15E+04
5.30E+04	2.10E+07	4.72E+07	1.04E+06	5.93E+07	9.76E+04
5.02E+04	1.57E+07	3.27E+07	1.02E+06	5.93E+07	7.31E+04
5.87E+04	1.94E+07	4.19E+07	1.05E+06	5.93E+07	9.63E+04
5.00E+04	1.67E+07	3.05E+07	2.74E+06	5.93E+07	8.75E+04
5.71E+04	1.63E+07	3.60E+07	8.85E+05	5.93E+07	7.68E+04
5.19E+04	1.11E+07	4.06E+07	3.06E+06	5.38E+07	5.05E+04
6.49E+04	1.54E+07	4.13E+07	7.58E+06	5.98E+07	8.15E+04
4.43E+04	1.32E+06	1.48E+07	3.35E+05	6.69E+06	2.12E+04
4.60E+04	2.95E+06	2.45E+07	4.40E+05	2.34E+07	2.85E+04
5.22E+04	1.40E+07	4.94E+07	1.28E+06	5.98E+07	1.13E+05
6.37E+04	1.79E+07	4.33E+07	8.75E+05	5.98E+07	1.02E+05
6.13E+04	1.10E+07	5.55E+07	6.88E+06	5.98E+07	1.03E+05
8.02E+04	1.45E+07	7.18E+06	2.38E+05	5.51E+07	5.94E+04
8.00E+04	1.58E+07	6.43E+06	2.36E+05	5.05E+07	5.54E+04
6.20E+04	1.01E+07	9.88E+06	9.11E+04	5.66E+07	1.91E+05
5.73E+04	1.02E+07	1.04E+07	1.57E+05	5.15E+07	1.33E+05
5.26E+04	7.08E+06	1.13E+07	1.21E+06	9.64E+06	1.43E+04
7.47E+04	1.62E+07	6.59E+06	1.48E+05	1.50E+07	2.20E+04
6.11E+04	1.02E+07	5.45E+06	1.42E+05	4.63E+07	6.26E+04
6.80E+04	1.16E+07	1.02E+07	1.15E+05	5.68E+07	1.89E+05
-8.81E+04	1.15E+07	6.86E+06	4.91E+04	6.95E+07	7.41E+03
-8.17E+04	1.52E+07	3.02E+07	1.01E+05	6.81E+07	1.65E+04

Sample	Analysis Name	X	Y	^{16}O (cps/nA)	^{18}O (cps/nA)	meas. $\delta^{18}O$ (‰)	1σ (‰)	mass 12.8 (cps)	^{12}CH (cps/nA)	^{16}O (cps/nA)	^{28}Si (cps/nA)	^{32}S (cps/nA)	^{56}FeO (cps/nA)
	PPRG134@04	736	-6533	6.70E+06	4.71E+03	-35.65	1.37	-8.75E+04	1.14E+07	5.78E+06	9.33E+04	6.88E+07	6.12E+03
	PPRG134@06	816	-6533	9.85E+06	1.08E+04	-26.60	1.02	-9.28E+04	1.39E+07	9.72E+06	6.30E+04	5.93E+07	5.32E+03
	PPRG134@09	936	-6533	1.68E+07	2.46E+04	-29.51	0.87	-8.19E+04	1.57E+07	2.00E+07	1.12E+05	6.95E+07	1.02E+04
	PPRG134@10	976	-6533	2.13E+07	3.39E+04	-24.18	0.52	-8.45E+04	1.34E+07	3.08E+07	7.25E+04	7.00E+07	1.74E+04
	PPRG134@11	976	-6613	1.87E+07	2.86E+04	-27.04	0.71	-8.50E+04	1.36E+07	1.26E+07	8.77E+04	6.94E+07	8.20E+03
	PPRG134@12	936	-6613	3.01E+07	5.13E+04	-27.44	0.46	-8.43E+04	1.46E+07	1.56E+07	7.27E+04	6.99E+07	9.73E+03
	PPRG134@13	896	-6613	2.89E+07	4.89E+04	-25.27	0.39	-8.38E+04	1.48E+07	1.77E+07	8.85E+04	6.96E+07	1.13E+04
	PPRG134@14	856	-6613	1.48E+07	2.07E+04	-23.89	0.76	-8.86E+04	1.40E+07	1.03E+07	7.34E+04	6.95E+07	5.46E+03
	PPRG134@15	816	-6613	1.56E+07	2.24E+04	-27.04	0.47	-8.43E+04	1.52E+07	2.68E+07	1.02E+05	6.90E+07	1.22E+04
	PPRG134@16	776	-6613	2.57E+07	4.25E+04	-25.53	0.53	-8.90E+04	1.39E+07	1.23E+07	6.49E+04	6.94E+07	7.54E+03
	PPRG134@17	736	-6613	7.58E+06	6.36E+03	-31.62	1.41	-9.28E+04	1.20E+07	6.14E+06	9.34E+04	4.97E+07	3.11E+03
	PPRG134@18	696	-6613	1.29E+07	1.70E+04	-25.10	0.68	-8.86E+04	1.32E+07	8.67E+06	8.21E+04	6.92E+07	8.31E+03
	PPRG134@19	656	-6613	2.46E+07	4.04E+04	-26.80	0.49	-8.31E+04	1.43E+07	2.28E+07	1.21E+05	6.82E+07	1.28E+04
	PPRG134@22	656	-6653	4.41E+07	7.90E+04	-28.05	0.26	-7.87E+04	6.70E+06	5.49E+07	3.98E+04	6.94E+07	1.93E+04
	PPRG134@23	696	-6653	1.87E+07	2.87E+04	-24.92	0.67	-8.31E+04	1.17E+07	1.84E+07	1.05E+05	7.06E+07	1.43E+04
	PPRG134@24	736	-6653	1.01E+07	1.13E+04	-28.26	1.01	-8.37E+04	8.40E+06	1.15E+07	7.95E+04	6.81E+07	9.30E+03
	PPRG134@25	776	-6653	1.26E+07	1.65E+04	-26.90	0.85	-8.59E+04	1.15E+07	1.14E+07	5.65E+04	6.98E+07	1.06E+04
	PPRG134@26	816	-6653	1.89E+07	2.92E+04	-25.86	0.73	-8.67E+04	1.39E+07	1.77E+07	7.42E+04	6.92E+07	9.84E+03
	PPRG134@27	856	-6653	1.40E+07	1.92E+04	-29.29	0.68	-8.36E+04	1.39E+07	2.09E+07	8.99E+04	6.84E+07	1.01E+04
	PPRG134@28	896	-6653	1.20E+07	1.52E+04	-29.17	0.85	-9.13E+04	1.37E+07	9.72E+06	7.50E+04	5.78E+07	4.40E+03
	PPRG134@29	936	-6653	8.44E+06	8.26E+03	-22.25	1.24	-8.67E+04	1.19E+07	1.01E+07	7.93E+04	6.91E+07	8.15E+03
	PPRG134@30	976	-6653	2.93E+07	4.97E+04	-26.49	0.45	-8.12E+04	1.49E+07	4.01E+07	1.57E+05	7.12E+07	1.89E+04
	PPRG134@31	976	-6733	1.88E+07	2.86E+04	-31.30	0.50	-8.31E+04	1.44E+07	2.55E+07	1.19E+05	7.10E+07	1.69E+04
	PPRG134@32	936	-6733	1.70E+07	2.53E+04	-23.80	0.61	-8.41E+04	1.33E+07	1.86E+07	8.71E+04	6.99E+07	1.08E+04
	PPRG134@33	896	-6733	1.21E+07	1.53E+04	-29.84	0.80	-8.67E+04	1.30E+07	1.13E+07	7.84E+04	6.98E+07	7.95E+03
	PPRG134@34	856	-6733	1.99E+07	3.10E+04	-22.51	0.57	-9.15E+04	1.33E+07	1.08E+07	7.83E+04	6.87E+07	5.17E+03
	PPRG134@35	816	-6733	1.29E+07	1.68E+04	-31.08	0.75	-8.59E+04	1.34E+07	1.32E+07	6.63E+04	6.96E+07	9.63E+03
	PPRG134@36	776	-6733	2.82E+07	4.74E+04	-26.94	0.49	-8.27E+04	1.50E+07	2.03E+07	5.39E+04	6.91E+07	1.36E+04
	PPRG134@37	736	-6733	3.12E+07	5.31E+04	-30.91	0.33	-8.45E+04	1.60E+07	2.13E+07	9.01E+04	7.01E+07	1.40E+04
	PPRG134@38	696	-6733	2.45E+07	3.96E+04	-37.42	0.52	-8.35E+04	1.10E+07	2.39E+07	5.51E+04	7.00E+07	1.55E+04
	PPRG134@39	656	-6733	1.59E+07	2.29E+04	-29.76	0.70	-8.51E+04	9.48E+06	1.25E+07	6.14E+04	6.94E+07	9.01E+03
	PPRG134@42	536	-6733	1.20E+07	1.53E+04	-20.89	1.21	-8.74E+04	1.15E+07	1.06E+07	8.18E+04	6.93E+07	6.26E+03

Sample	Analysis Name	X	Y	^{16}O (cps/nA)	^{18}O (cps/nA)	meas. $\delta^{18}O$ (‰)	1σ (‰)	mass 12.8 (cps)	^{12}CH (cps/nA)	^{16}O (cps/nA)	^{28}Si (cps/nA)	^{32}S (cps/nA)	^{56}FeO (cps/nA)
	PPRG134@43	496	-6733	1.44E+07	1.99E+04	-27.18	0.90	-8.61E+04	1.16E+07	1.11E+07	1.17E+05	6.92E+07	8.19E+03
	PPRG134@45	416	-6733	2.36E+07	3.77E+04	-41.90	0.66	-8.36E+04	6.03E+06	1.55E+07	5.45E+04	6.67E+07	8.98E+03
Nabberu	Naberu@1	1816	240	9.42E+06	2.83E+04	-9.42	1.00	4.95E+04	6.42E+06	4.97E+06	3.83E+04	2.25E+06	8.17E+03
PPRG 089	Naberu@02	1856	240	7.57E+06	2.47E+04	-11.83	1.19	5.21E+04	1.17E+07	4.62E+06	9.98E+04	4.11E+06	8.76E+03
	Naberu@03	1778	230	1.11E+07	3.16E+04	-9.52	0.77	4.89E+04	3.84E+06	3.67E+06	2.41E+04	1.61E+06	7.57E+03
	Naberu@04	1710	230	9.94E+06	2.97E+04	-3.48	1.06	5.16E+04	4.40E+06	3.99E+06	4.55E+04	1.73E+06	6.01E+03
	Naberu@05	1739	294	9.02E+06	2.77E+04	-14.97	1.12	4.43E+04	3.43E+06	3.06E+06	2.08E+04	1.63E+06	6.15E+03
	Naberu@06	1821	285	9.07E+06	2.79E+04	-10.67	1.17	5.42E+04	9.09E+06	4.99E+06	6.33E+04	3.07E+06	7.19E+03
	Naberu@07	1905	283	8.58E+06	2.67E+04	-14.01	0.95	6.36E+04	1.36E+07	4.78E+06	4.61E+05	3.94E+06	7.62E+03
	Naberu@08	1988	278	9.72E+06	2.89E+04	-15.79	0.95	4.71E+04	8.81E+06	4.57E+06	7.80E+04	2.38E+06	6.79E+03
	Naberu@09	2078	272	6.35E+06	2.24E+04	-6.97	1.50	5.11E+04	8.91E+06	2.89E+06	1.18E+05	3.44E+06	7.10E+03
	Naberu@10	2127	346	7.97E+06	2.57E+04	-4.24	1.03	5.98E+04	1.17E+07	3.84E+06	1.19E+05	3.06E+06	6.52E+03
	Naberu@11	2042	394	8.54E+06	2.68E+04	-12.97	1.03	6.09E+04	1.35E+07	5.81E+06	9.36E+04	3.03E+06	8.91E+03
	Naberu@12	1925	402	8.51E+06	2.69E+04	-6.01	1.01	7.59E+04	6.67E+06	5.03E+06	9.75E+04	2.15E+06	8.78E+03
	Naberu@13	1956	450	7.75E+06	2.53E+04	-10.65	0.96	4.53E+04	4.10E+06	3.84E+06	2.10E+04	1.51E+06	6.60E+03
	Naberu@14	2039	505	8.15E+06	2.61E+04	-15.21	1.10	5.46E+04	9.18E+06	4.60E+06	1.03E+05	2.28E+06	6.27E+03
	Naberu@15	1960	530	8.77E+06	2.74E+04	-4.75	0.85	7.53E+04	1.43E+07	6.32E+06	1.20E+05	4.95E+06	1.07E+04
	Naberu@16	1872	558	7.58E+06	2.49E+04	-0.99	1.48	5.65E+04	1.17E+07	4.34E+06	1.24E+05	3.74E+06	7.83E+03
	Naberu@17	1975	580	7.87E+06	2.53E+04	-7.18	1.09	5.22E+04	4.08E+06	3.99E+06	2.35E+04	1.54E+06	7.37E+03
	Naberu@18	2077	589	7.34E+06	2.46E+04	0.21	1.15	6.01E+04	1.08E+07	4.75E+06	9.04E+04	3.28E+06	7.85E+03
	Naberu@19	2146	644	1.34E+07	3.62E+04	-16.89	0.77	1.02E+05	1.41E+07	6.00E+06	1.11E+05	4.18E+06	8.95E+03
	Naberu@20	2182	710	1.02E+07	3.01E+04	-9.49	0.93	5.14E+04	9.47E+06	4.74E+06	8.30E+04	3.55E+06	9.73E+03
	Naberu@21	2163	833	7.36E+06	2.47E+04	-3.96	0.99	7.41E+04	1.27E+07	3.39E+06	1.26E+05	6.58E+06	7.94E+03
	Naberu@22	2108	880	7.32E+06	2.45E+04	-4.54	1.09	8.51E+04	1.32E+07	5.04E+06	3.04E+05	4.97E+06	9.18E+03
	Naberu@23	2100	946	7.17E+06	2.43E+04	-6.32	1.18	7.44E+04	1.18E+07	3.80E+06	1.92E+05	4.47E+06	1.08E+04
	Naberu@24	2214	991	8.15E+06	2.63E+04	-2.06	0.82	7.14E+04	1.40E+07	5.27E+06	1.36E+05	5.49E+06	9.19E+03
	Naberu@25	2369	1226	7.15E+06	2.42E+04	-7.78	1.45	7.09E+04	1.10E+07	3.84E+06	9.53E+04	4.61E+06	7.12E+03
Wabigoon	Wabigoon@1	4287	-222	3.98E+07	9.98E+04	-6.84	0.39	4.17E+04	4.73E+06	2.35E+07	9.46E+03	1.20E+07	2.80E+04
PPRG 325	Wabigoon@02	4327	-222	2.26E+07	6.61E+04	-3.61	1.05	3.54E+04	2.21E+06	1.44E+07	8.21E+03	8.30E+06	1.99E+04
	Wabigoon@03	4367	-222	1.22E+07	4.53E+04	-13.60	1.29	3.56E+04	1.13E+06	5.20E+06	7.92E+03	1.48E+06	1.07E+04
	Wabigoon@04	4407	-222	5.49E+07	1.30E+05	-4.58	0.32	3.84E+04	5.97E+06	3.88E+07	1.06E+04	1.01E+07	4.71E+04
	Wabigoon@05	4447	-222	4.28E+07	1.07E+05	1.49	0.49	3.76E+04	7.78E+05	4.16E+06	7.93E+03	1.46E+06	1.08E+04

Sample	Analysis Name	X	Y	^{16}O (cps/nA)	^{18}O (cps/nA)	meas. $\delta^{18}O$ (‰)	1σ (‰)	mass 12.8 (cps)	^{12}CH (cps/nA)	^{16}O (cps/nA)	^{28}Si (cps/nA)	^{32}S (cps/nA)	^{56}FeO (cps/nA)
	Wabigoon@07	4527	-222	5.62E+07	1.32E+05	-2.25	0.37	3.54E+04	5.30E+06	4.33E+07	1.03E+04	1.41E+07	5.46E+04
	Wabigoon@08	4567	-222	5.80E+07	1.36E+05	-1.24	0.40	3.69E+04	4.51E+06	4.54E+07	9.97E+03	6.82E+06	4.65E+04
	Wabigoon@09	4607	-222	2.87E+07	7.78E+04	-4.68	0.61	3.82E+04	1.72E+06	1.52E+07	8.79E+03	3.69E+06	1.76E+04
	Wabigoon@10	4647	-222	6.01E+07	1.41E+05	-0.88	0.27	3.92E+04	4.84E+06	3.30E+07	1.06E+04	2.04E+07	4.60E+04
	Wabigoon@11	4647	-182	5.06E+07	1.21E+05	-8.45	0.37	3.59E+04	3.16E+06	2.84E+07	9.20E+03	8.27E+06	2.75E+04
	Wabigoon@12	4607	-182	5.60E+07	1.32E+05	-1.83	0.39	3.54E+04	1.59E+06	1.57E+07	8.39E+03	6.40E+06	1.98E+04
	Wabigoon@13	4567	-182	5.52E+07	1.31E+05	-1.61	0.31	3.75E+04	4.63E+06	3.29E+07	1.01E+04	1.78E+07	4.00E+04
	Wabigoon@14	4527	-182	6.35E+07	1.47E+05	-2.65	0.28	3.60E+04	4.58E+06	3.80E+07	1.02E+04	7.77E+06	4.89E+04
	Wabigoon@17	4407	-182	7.12E+07	1.63E+05	-1.40	0.30	3.71E+04	4.63E+06	3.35E+07	9.80E+03	7.88E+06	2.76E+04
	Wabigoon@18	4367	-182	5.05E+07	1.21E+05	-4.15	0.33	3.69E+04	4.59E+06	1.61E+07	1.00E+04	1.77E+07	2.57E+04
	Wabigoon@19	4327	-182	4.39E+07	1.07E+05	-8.81	0.40	3.72E+04	5.26E+06	2.76E+07	1.06E+04	5.23E+06	3.33E+04
	Wabigoon@20	4287	-182	4.60E+07	1.12E+05	-6.55	0.40	3.81E+04	2.87E+06	1.57E+07	8.89E+03	5.16E+06	1.85E+04
	Wabigoon@21	4247	-182	6.40E+07	1.48E+05	-2.74	0.22	3.71E+04	6.13E+06	3.62E+07	1.03E+04	8.71E+06	3.83E+04
	Wabigoon@23	4207	-142	5.64E+07	1.33E+05	-5.18	0.38	3.87E+04	4.28E+06	2.47E+07	9.95E+03	7.14E+06	3.21E+04
	Wabigoon@24	4207	-102	3.89E+07	9.82E+04	-5.45	0.62	3.89E+04	3.55E+06	3.03E+07	9.92E+03	4.71E+06	3.58E+04
	Wabigoon@25	4207	-62	4.53E+07	1.11E+05	-1.65	0.42	3.74E+04	4.87E+06	1.48E+07	9.53E+03	6.83E+06	2.28E+04
	Wabigoon@26	4207	-22	6.29E+07	1.46E+05	0.22	0.40	3.65E+04	5.80E+06	2.89E+07	1.01E+04	9.41E+06	3.60E+04
	Wabigoon@27	4207	18	9.08E+07	2.02E+05	3.37	0.24	3.67E+04	2.45E+06	4.08E+07	9.03E+03	5.86E+06	3.32E+04
	Wabigoon@28	4207	58	4.94E+07	1.19E+05	-4.65	0.39	3.78E+04	6.95E+06	2.86E+07	1.05E+04	2.85E+07	4.02E+04
	Wabigoon@29	4207	98	3.41E+07	8.85E+04	-4.41	0.44	3.64E+04	1.98E+06	9.18E+06	8.73E+03	1.97E+06	1.23E+04
	Wabigoon@30	4207	138	5.17E+07	1.23E+05	-9.53	0.31	3.68E+04	4.58E+06	1.77E+07	9.93E+03	3.47E+06	2.09E+04
	Wabigoon@31	4207	178	4.81E+07	1.16E+05	-4.52	0.42	3.84E+04	5.14E+06	3.07E+07	1.09E+04	8.87E+06	3.88E+04
	Wabigoon@32	4207	218	3.01E+07	8.11E+04	-5.03	0.52	3.75E+04	5.21E+06	1.57E+07	9.75E+03	1.04E+07	2.73E+04
Farrel Quartzite MGTKS1	MGTKS1@50	-1917	-1297	2.30E+07	4.56E+04	-13.08	0.28	3.91E+04	1.71E+07	3.51E+07	2.13E+06	1.18E+07	2.14E+04
	MGTKS1@51	-1917	-1247	3.86E+07	7.64E+04	-9.36	0.26	4.50E+04	1.16E+07	4.56E+07	2.30E+06	5.90E+07	4.38E+04
	MGTKS1@52	-1917	-1197	1.05E+08	2.07E+05	-5.49	0.07	4.02E+04	5.86E+06	1.27E+08	6.00E+06	5.41E+07	1.01E+05
	MGTKS1@53	-1917	-1147	2.51E+07	5.00E+04	-10.27	0.41	3.83E+04	1.06E+07	1.30E+07	3.02E+05	1.87E+07	2.76E+04
	MGTKS1@54	-1917	-1097	3.15E+07	6.25E+04	-12.42	0.24	4.20E+04	1.43E+07	1.42E+07	1.08E+05	1.05E+07	1.09E+04
	MGTKS1@55	-1917	-1047	1.57E+07	3.14E+04	-18.17	0.39	3.98E+04	1.26E+07	8.33E+06	5.46E+04	6.96E+06	1.07E+04
	MGTKS1@56	-1917	-997	1.75E+07	3.49E+04	-14.36	0.35	4.07E+04	1.33E+07	7.92E+06	6.62E+04	7.05E+06	1.33E+04
	MGTKS1@57	-1917	-947	2.24E+07	4.48E+04	-14.10	0.26	4.02E+04	1.40E+07	9.17E+06	1.25E+05	7.42E+06	1.77E+04
	MGTKS1@58	-1917	-897	5.33E+07	1.06E+05	-10.60	0.17	4.14E+04	1.68E+07	6.53E+07	2.99E+06	6.02E+07	7.96E+04

Sample	Analysis Name	X	Y	^{16}O (cps/nA)	^{18}O (cps/nA)	meas. $\delta^{18}O$ (‰)	1σ (‰)	mass 12.8 (cps)	^{12}CH (cps/nA)	^{16}O (cps/nA)	^{28}Si (cps/nA)	^{32}S (cps/nA)	^{56}FeO (cps/nA)
	MGTKS1@60	-1917	-797	3.96E+07	7.85E+04	-11.24	0.21	4.67E+04	1.30E+07	7.06E+07	3.70E+06	8.67E+07	7.71E+04
	MGTKS1@61	-1917	-747	5.29E+07	1.05E+05	-9.03	0.18	4.60E+04	1.37E+07	4.76E+07	3.75E+06	1.35E+08	5.85E+04
	MGTKS1@62	-1917	-697	8.83E+07	1.75E+05	-6.84	0.10	4.60E+04	1.53E+07	7.98E+07	4.48E+06	2.47E+08	1.14E+05
	MGTKS1@64	-1917	-597	3.91E+07	7.77E+04	-8.39	0.23	4.58E+04	1.98E+07	5.22E+07	2.43E+06	6.78E+07	5.14E+04
	MGTKS1@65	-1867	-597	8.62E+07	1.70E+05	-10.62	0.21	4.39E+04	1.54E+07	8.61E+07	2.29E+06	7.29E+07	5.01E+04
	MGTKS1@66	-1817	-597	7.53E+07	1.49E+05	-7.98	0.24	4.52E+04	1.72E+07	5.57E+07	2.64E+06	9.24E+07	6.77E+04
	MGTKS1@67	-1767	-597	8.17E+07	1.61E+05	-9.74	0.14	4.46E+04	1.47E+07	2.60E+08	1.09E+07	7.20E+07	1.40E+05
	MGTKS1@68	-1717	-597	9.40E+07	1.87E+05	-3.56	0.14	4.46E+04	8.87E+06	8.11E+07	1.99E+06	2.64E+07	2.30E+04
	MGTKS1@69	-1667	-597	7.09E+07	1.40E+05	-9.57	0.13	4.40E+04	1.41E+07	1.41E+08	8.83E+06	8.30E+07	1.12E+05
	MGTKS1@70	-1667	-647	1.62E+07	3.28E+04	-10.66	0.42	4.03E+04	7.27E+06	1.10E+07	2.81E+04	3.52E+06	6.14E+03
	MGTKS1@71	-1667	-697	4.75E+07	9.45E+04	-7.91	0.26	4.08E+04	7.83E+06	3.35E+07	1.55E+06	3.81E+07	2.49E+04
	MGTKS1@72	-1667	-747	5.74E+07	1.14E+05	-9.97	0.15	4.49E+04	1.54E+07	2.13E+08	1.14E+07	7.60E+07	3.10E+05
	MGTKS1@73	-1667	-797	1.65E+07	3.31E+04	-15.72	0.58	3.93E+04	1.02E+07	6.96E+06	2.01E+04	4.47E+06	5.95E+03
	MGTKS1@74	-1667	-847	2.50E+07	5.01E+04	-10.16	0.36	4.05E+04	8.93E+06	8.93E+06	5.21E+05	9.01E+06	8.54E+03
	MGTKS1@75	-1617	-847	2.70E+08	5.34E+05	-5.65	0.07	4.47E+04	3.95E+06	3.50E+08	1.84E+07	4.35E+08	4.89E+05
	MGTKS1@76	-1567	-847	1.44E+08	2.84E+05	-4.69	0.07	4.04E+04	1.04E+07	1.66E+08	8.11E+06	4.65E+07	1.02E+05
	MGTKS1@77	-1517	-847	6.54E+07	1.29E+05	-8.85	0.18	4.03E+04	9.44E+06	5.64E+07	3.43E+06	5.32E+07	5.08E+04
	MGTKS1@78	-1467	-847	4.47E+07	8.89E+04	-7.21	0.22	4.53E+04	1.30E+07	3.31E+07	2.99E+06	7.16E+07	3.87E+04
	MGTKS1@79	-1417	-847	4.47E+07	8.89E+04	-7.26	0.34	4.37E+04	1.14E+07	3.68E+07	2.07E+06	1.16E+08	4.52E+04
	MGTKS1@81	-1417	-747	3.36E+07	6.65E+04	-14.42	0.26	4.02E+04	1.75E+07	1.36E+07	2.56E+05	1.96E+07	1.26E+04
	MGTKS1@82	-1417	-697	2.32E+07	4.61E+04	-15.65	0.23	4.05E+04	1.33E+07	9.28E+06	5.58E+04	7.68E+06	8.48E+03
	MGTKS1@83	-1417	-647	3.99E+07	7.92E+04	-11.76	0.20	4.24E+04	1.81E+07	4.50E+07	2.43E+06	5.79E+07	4.57E+04
	MGTKS1@85	-1417	-547	1.86E+07	3.73E+04	-13.69	0.36	4.03E+04	1.07E+07	8.17E+06	3.95E+05	2.87E+07	9.27E+03
	MGTKS1@86	-1417	-497	1.09E+08	2.15E+05	-5.42	0.09	4.35E+04	1.59E+07	3.51E+07	2.47E+06	5.56E+07	3.57E+04
	MGTKS1@87	-1417	-447	6.14E+07	1.22E+05	-6.96	0.13	4.22E+04	7.87E+06	8.88E+07	4.77E+06	1.15E+08	1.12E+05
	MGTKS1@88	-1417	-397	5.65E+07	1.11E+05	-11.63	0.18	4.42E+04	1.38E+07	8.25E+07	4.55E+06	6.49E+07	7.86E+04
	MGTKS1@89	-1417	-347	6.38E+07	1.27E+05	-7.43	0.14	4.30E+04	1.63E+07	4.43E+07	3.06E+06	5.54E+07	4.76E+04
Farrel Quartzite MGTKS1	MGTKS1@02	-70	2401	2.47E+07	4.19E+04	-6.00	0.53	-8.83E+04	7.63E+06	2.47E+07	1.88E+06	3.31E+07	2.68E+03
	MGTKS1@03	-20	2401	3.96E+07	7.23E+04	-2.68	0.44	-7.95E+04	7.76E+06	2.82E+07	1.76E+06	6.49E+07	8.12E+03
	MGTKS1@04	30	2401	4.38E+07	8.03E+04	-9.54	0.31	-8.55E+04	8.32E+06	4.12E+07	2.68E+06	3.61E+07	2.38E+03
	MGTKS1@05	80	2401	4.45E+07	8.22E+04	-3.63	0.13	-8.61E+04	7.64E+06	3.92E+07	3.39E+06	4.14E+07	3.51E+03
	MGTKS1@06	130	2401	1.16E+07	1.52E+04	-7.27	0.67	-9.88E+04	6.43E+06	4.17E+06	1.54E+05	4.17E+06	-3.38E+02

Sample	Analysis Name	X	Y	^{16}O (cps/nA)	^{18}O (cps/nA)	meas. $\delta^{18}O$ (‰)	1σ (‰)	mass 12.8 (cps)	^{12}CH (cps/nA)	^{16}O (cps/nA)	^{28}Si (cps/nA)	^{32}S (cps/nA)	^{56}FeO (cps/nA)
	MGTKS1@07	180	2401	4.12E+07	7.54E+04	-5.48	0.31	-8.70E+04	9.96E+06	2.78E+07	1.39E+06	6.06E+07	5.77E+03
	MGTKS1@08	230	2401	3.16E+07	5.59E+04	-5.09	0.59	-9.02E+04	8.38E+06	1.63E+07	1.34E+06	3.67E+07	1.69E+03
	MGTKS1@09	280	2401	3.26E+07	5.78E+04	-3.61	0.52	-9.35E+04	5.73E+06	1.60E+07	1.53E+06	1.17E+07	1.05E+03
	MGTKS1@10	330	2401	1.93E+07	3.08E+04	-7.66	0.46	-9.27E+04	5.97E+06	1.13E+07	1.46E+06	4.20E+07	3.21E+03
	MGTKS1@11	330	2451	2.57E+07	4.40E+04	-6.46	0.24	-8.88E+04	7.31E+06	3.49E+07	5.93E+06	3.81E+07	3.84E+03
	MGTKS1@14	180	2451	1.83E+07	2.90E+04	-3.19	0.69	-9.32E+04	5.67E+06	1.95E+07	2.74E+06	2.15E+07	1.97E+03
	MGTKS1@15	130	2451	1.25E+07	1.70E+04	-6.87	0.79	-9.63E+04	6.23E+06	7.18E+06	2.02E+05	6.50E+06	-8.74E+01
	MGTKS1@16	80	2451	3.89E+07	7.00E+04	-15.81	0.37	-8.26E+04	5.21E+06	1.47E+07	5.28E+05	6.82E+07	1.16E+04
	MGTKS1@17	30	2451	3.26E+07	5.81E+04	0.07	0.46	-9.21E+04	7.33E+06	1.81E+07	1.37E+06	2.70E+07	1.23E+03
	MGTKS1@18	-20	2451	3.28E+07	5.84E+04	-3.43	0.36	-8.89E+04	7.84E+06	2.85E+07	2.52E+06	3.19E+07	2.87E+03
	MGTKS1@20	-120	2451	1.95E+07	3.13E+04	-2.67	0.47	-8.61E+04	7.44E+06	4.65E+07	4.69E+06	2.84E+07	2.50E+03
	MGTKS1@21	-120	2501	1.43E+07	2.04E+04	-10.89	0.78	-9.12E+04	9.01E+06	1.89E+07	2.06E+06	4.40E+07	3.15E+03
	MGTKS1@22	-70	2501	3.58E+07	6.43E+04	-5.63	0.28	-8.03E+04	8.40E+06	3.02E+07	3.13E+06	6.16E+07	5.85E+03
	MGTKS1@23	-20	2501	3.88E+07	7.02E+04	-9.49	0.17	-8.83E+04	8.11E+06	1.36E+07	7.75E+05	3.63E+07	1.74E+03
	MGTKS1@24	30	2501	4.30E+07	7.92E+04	-2.83	0.25	-7.78E+04	5.84E+06	6.15E+07	4.47E+06	6.18E+07	7.06E+03
	MGTKS1@25	80	2501	2.00E+07	3.20E+04	-7.57	0.53	-8.52E+04	6.62E+06	1.61E+07	8.33E+05	6.78E+07	4.21E+03
	MGTKS1@27	180	2501	2.11E+07	3.47E+04	-4.92	0.35	-9.21E+04	8.97E+06	1.46E+07	1.03E+06	3.25E+07	2.46E+03
	MGTKS1@28	230	2501	2.58E+07	4.42E+04	-6.31	0.44	-9.09E+04	7.09E+06	1.86E+07	1.39E+06	4.26E+07	3.47E+03
	MGTKS1@29	280	2501	2.74E+07	4.75E+04	-5.96	0.37	-8.67E+04	7.24E+06	2.79E+07	2.18E+06	3.95E+07	2.66E+03
	MGTKS1@30	330	2501	2.92E+07	5.07E+04	-9.43	0.38	-8.83E+04	7.04E+06	2.56E+07	2.14E+06	3.94E+07	2.63E+03
	MGTKS1@31	330	2551	4.22E+07	7.73E+04	-8.13	0.29	-7.82E+04	5.79E+06	6.57E+07	6.12E+06	3.08E+07	3.60E+03
	MGTKS1@32	280	2551	2.05E+07	3.33E+04	-7.29	0.66	-8.67E+04	7.95E+06	3.25E+07	2.25E+06	4.27E+07	2.75E+03
	MGTKS1@33	230	2551	2.85E+07	4.97E+04	-4.83	0.36	-8.58E+04	7.80E+06	2.96E+07	3.20E+06	4.71E+07	3.57E+03
	MGTKS1@34	180	2551	2.48E+07	4.20E+04	-7.87	0.60	-8.79E+04	7.31E+06	1.56E+07	1.63E+06	4.71E+07	3.00E+03
	MGTKS1@35	130	2551	5.68E+07	1.08E+05	0.81	0.25	-7.76E+04	5.03E+06	6.61E+07	7.27E+06	2.75E+07	3.98E+03
	MGTKS1@36	80	2551	2.48E+07	4.22E+04	-6.23	0.37	-7.98E+04	6.89E+06	2.24E+07	2.67E+06	6.54E+07	5.72E+03
	MGTKS1@39	-70	2551	4.82E+07	8.99E+04	-3.52	0.25	-7.97E+04	6.83E+06	3.19E+07	1.62E+06	6.46E+07	5.69E+03
	MGTKS1@40	-120	2551	2.36E+07	3.96E+04	-6.41	0.42	-8.71E+04	8.83E+06	1.96E+07	1.53E+06	5.66E+07	3.87E+03
	MGTKS1@41	-170	2551	6.49E+07	1.24E+05	-1.16	0.16	-7.67E+04	4.11E+06	6.61E+07	1.07E+07	2.06E+07	3.28E+03
	MGTKS1@42	-220	2551	2.69E+07	4.64E+04	-4.66	0.42	-8.43E+04	7.78E+06	2.13E+07	1.70E+06	5.90E+07	5.04E+03
Josefsdal	Josefsdal@01	361	773	2.66E+08	5.29E+05	-9.45	0.11	-8.40E+04	5.59E+06	5.55E+08	9.73E+05	2.38E+08	2.79E+04
99SA07	Josefsdal@02	411	773	2.66E+08	5.30E+05	-9.85	0.10	-8.94E+04	7.82E+06	4.34E+08	7.52E+05	2.34E+08	1.57E+04

Sample	Analysis Name	X	Y	^{16}O (cps/nA)	^{18}O (cps/nA)	meas. $\delta^{18}O$ (‰)	1σ (‰)	mass 12.8 (cps)	^{12}CH (cps/nA)	^{16}O (cps/nA)	^{28}Si (cps/nA)	^{32}S (cps/nA)	^{56}FeO (cps/nA)
	Josefsdal@03	461	773	2.98E+08	5.95E+05	-8.74	0.12	-8.64E+04	4.36E+06	4.65E+08	1.62E+06	4.44E+08	2.85E+04
	Josefsdal@05	561	773	2.39E+08	4.76E+05	-9.15	0.11	-8.77E+04	3.94E+06	5.62E+08	4.94E+05	1.42E+08	1.64E+04
	Josefsdal@06	611	773	2.60E+08	5.18E+05	-10.29	0.13	-8.98E+04	5.16E+06	3.36E+08	7.14E+05	3.39E+08	1.98E+04
	Josefsdal@07	661	773	2.85E+08	5.68E+05	-9.06	0.06	-8.62E+04	2.95E+06	5.74E+08	5.08E+05	1.51E+08	1.26E+04
	Josefsdal@08	711	773	2.92E+08	5.84E+05	-6.51	0.15	-8.55E+04	2.00E+06	6.02E+08	2.62E+06	8.76E+07	1.30E+04
	Josefsdal@09	711	823	3.04E+08	6.09E+05	-6.76	0.23	-8.73E+04	2.71E+06	5.99E+08	5.07E+05	1.72E+08	1.38E+04
	Josefsdal@10	661	823	2.20E+08	4.36E+05	-9.94	0.08	-8.66E+04	5.40E+06	4.23E+08	6.28E+05	2.79E+08	1.79E+04
	Josefsdal@11	611	823	2.23E+08	4.42E+05	-10.49	0.10	-8.60E+04	3.46E+06	5.47E+08	7.48E+05	1.21E+08	1.23E+04
	Josefsdal@12	561	823	2.80E+08	5.57E+05	-11.07	0.11	-8.60E+04	3.47E+06	4.61E+08	1.10E+06	3.47E+08	2.34E+04
	Josefsdal@13	511	823	2.92E+08	5.83E+05	-7.79	0.14	-8.50E+04	3.91E+06	5.62E+08	4.37E+05	3.17E+08	2.02E+04
	Josefsdal@14	461	823	2.53E+08	5.02E+05	-10.75	0.07	-8.65E+04	4.20E+06	5.18E+08	7.39E+05	1.91E+08	1.53E+04
	Josefsdal@15	411	823	2.56E+08	5.07E+05	-11.59	0.10	-8.74E+04	8.28E+06	4.07E+08	1.01E+06	1.53E+08	1.23E+04
	Josefsdal@16	361	823	2.42E+08	4.80E+05	-10.56	0.16	-8.83E+04	7.65E+06	5.16E+08	1.37E+06	1.52E+08	1.70E+04
	Josefsdal@17	361	873	2.33E+08	4.62E+05	-10.28	0.09	-9.16E+04	1.14E+06	2.75E+08	1.24E+05	1.30E+08	8.93E+03
	Josefsdal@18	411	873	2.63E+08	5.23E+05	-10.02	0.11	-8.85E+04	5.76E+06	5.47E+08	7.34E+05	2.87E+08	2.02E+04
	Josefsdal@19	461	873	3.21E+08	6.40E+05	-11.94	0.13	-8.61E+04	8.36E+06	4.38E+08	8.30E+05	3.83E+08	2.51E+04
	Josefsdal@20	511	873	2.92E+08	5.84E+05	-8.67	0.25	-8.14E+04	3.17E+06	6.06E+08	1.33E+06	8.73E+07	1.62E+04
	Josefsdal@21	561	873	2.36E+08	4.68E+05	-10.54	0.12	-8.60E+04	2.99E+06	5.50E+08	6.89E+06	1.66E+08	1.23E+04
	Josefsdal@22	611	873	2.90E+08	5.79E+05	-9.49	0.07	-8.34E+04	3.14E+06	5.73E+08	1.34E+06	2.92E+08	1.94E+04
	Josefsdal@23	661	873	2.39E+08	4.76E+05	-8.91	0.16	-8.81E+04	6.29E+06	4.11E+08	6.90E+05	2.49E+08	1.83E+04
	Josefsdal@24	711	873	2.11E+08	4.21E+05	-1.42	0.10	-8.59E+04	2.48E+06	4.94E+08	3.02E+06	2.39E+08	1.34E+04
	Josefsdal@25	711	923	2.54E+08	5.07E+05	-7.63	0.10	-8.93E+04	5.57E+06	4.52E+08	1.30E+06	2.59E+08	1.67E+04
	Josefsdal@26	661	923	2.44E+08	4.84E+05	-8.80	0.08	-9.02E+04	6.89E+06	4.06E+08	1.87E+06	1.77E+08	1.32E+04
	Josefsdal@27	611	923	2.67E+08	5.31E+05	-9.26	0.26	-8.71E+04	6.45E+06	3.95E+08	7.12E+05	1.96E+08	1.54E+04
	Josefsdal@28	561	923	2.25E+08	4.47E+05	-10.17	0.19	-8.68E+04	4.63E+06	4.87E+08	6.54E+05	1.72E+08	1.26E+04
	Josefsdal@29	511	923	3.55E+08	7.11E+05	-8.42	0.11	-8.45E+04	4.40E+06	5.70E+08	6.86E+05	2.55E+08	2.03E+04
Buck Reef 99SA03	Buck@01	5211	-590	2.73E+07	4.73E+04	-8.70	0.71	-7.87E+04	8.81E+06	6.48E+07	1.20E+07	1.24E+07	5.95E+04
	Buck@03	5131	-590	9.92E+06	1.18E+04	-10.31	1.18	-9.86E+04	9.30E+06	7.77E+06	9.77E+04	1.49E+07	9.54E+03
	Buck@05	5051	-590	1.67E+07	2.57E+04	-11.36	0.66	-9.55E+04	1.11E+07	7.66E+06	3.83E+04	1.59E+07	1.96E+04
	Buck@06	5011	-590	2.13E+07	3.51E+04	-5.21	0.70	-9.54E+04	9.74E+06	8.26E+06	1.05E+05	1.59E+07	1.65E+04
	Buck@07	4971	-590	1.98E+07	3.17E+04	-10.93	0.74	-9.71E+04	8.93E+06	3.64E+06	5.71E+04	1.46E+07	6.44E+03
	Buck@08	4931	-590	7.06E+07	1.35E+05	-8.82	0.17	-9.15E+04	1.10E+07	2.30E+07	1.51E+05	1.61E+07	2.21E+04

Sample	Analysis Name	X	Y	^{16}O (cps/nA)	^{18}O (cps/nA)	meas. $\delta^{18}O$ (‰)	1σ (‰)		mass 12.8 (cps)	^{12}CH (cps/nA)	^{16}O (cps/nA)	^{28}Si (cps/nA)	^{32}S (cps/nA)	^{56}FeO (cps/nA)
	Buck@11	5011	-630	1.92E+07	3.09E+04	-6.36	0.55		-9.21E+04	9.41E+06	1.57E+07	7.20E+05	2.11E+07	1.71E+04
	Buck@13	5091	-630	1.71E+07	2.65E+04	-9.52	0.62		-9.23E+04	1.31E+07	1.01E+07	1.58E+05	2.30E+07	3.23E+04
	Buck@14	5131	-630	3.69E+07	6.62E+04	-13.64	0.48		-9.57E+04	1.03E+07	4.10E+06	8.83E+04	1.76E+07	8.32E+03
	Buck@16	5211	-630	1.25E+07	1.68E+04	-10.94	0.94		-9.50E+04	8.48E+06	6.21E+06	2.17E+05	1.74E+07	8.25E+03
	Buck@18	5171	-750	1.39E+07	1.98E+04	-12.59	0.81		-9.77E+04	8.23E+06	9.08E+06	2.37E+05	1.40E+07	8.38E+03
	Buck@19	5131	-750	1.19E+07	1.58E+04	-8.33	0.70		-9.16E+04	1.10E+07	3.14E+07	3.79E+05	1.54E+07	4.67E+04
	Buck@20	5091	-750	1.12E+07	1.44E+04	-9.74	1.02		-9.45E+04	1.30E+07	8.75E+06	9.20E+04	1.71E+07	2.01E+04
	Buck@21	5051	-750	1.05E+07	1.30E+04	-14.17	0.84		-9.73E+04	8.94E+06	7.37E+06	4.35E+04	1.71E+07	1.39E+04
	Buck@22	5011	-750	2.11E+07	3.46E+04	-9.01	0.60		-9.55E+04	1.03E+07	1.12E+07	3.08E+05	1.64E+07	1.63E+04
	Buck@23	4971	-750	1.13E+07	1.46E+04	-11.88	0.85		-9.66E+04	9.26E+06	7.38E+06	7.14E+04	1.42E+07	1.31E+04
	Buck@26	4851	-750	1.12E+07	1.43E+04	-12.62	1.00		-9.71E+04	9.68E+06	5.23E+06	2.32E+05	1.56E+07	8.03E+03
	Buck@27	4851	-710	3.21E+07	5.74E+04	-1.62	0.44		-9.64E+04	8.77E+06	8.31E+06	2.64E+05	1.40E+07	1.08E+04
	Buck@28	4851	-670	1.45E+07	2.11E+04	-6.73	0.80		-9.66E+04	9.63E+06	6.53E+06	1.87E+05	1.64E+07	2.26E+04
	Buck@29	4851	-630	1.40E+07	1.99E+04	-19.16	0.62		-9.34E+04	9.49E+06	1.05E+07	7.21E+04	2.73E+07	1.72E+04
	Buck@31	4851	-550	1.54E+07	2.29E+04	-12.57	0.47		-9.68E+04	1.19E+07	9.77E+06	6.72E+04	1.38E+07	1.72E+04
	Buck@33	4851	-470	1.93E+07	3.05E+04	-13.99	0.64		-9.47E+04	1.07E+07	1.48E+07	2.73E+05	1.40E+07	2.82E+04
	Buck@34	4851	-430	1.50E+07	2.21E+04	-12.53	1.10		-9.76E+04	8.82E+06	7.47E+06	5.69E+04	1.21E+07	1.19E+04
	Buck@35	4851	-390	6.26E+07	1.20E+05	-2.24	0.27		-8.51E+04	6.72E+06	5.35E+07	3.37E+06	9.83E+06	2.45E+04
	Buck@36	4851	-350	1.13E+07	1.45E+04	-12.83	1.01		-9.68E+04	8.62E+06	8.97E+06	8.59E+04	1.31E+07	1.20E+04

Table S-5 Final SIMS O isotope dataset.

Sample	Analysis Name	Age (Ma)	Bulk $\delta^{18}O$ (‰)	$\delta^{18}O$ corr. IMF (‰)	2σ (‰)
Doushantuo 1a of 8/25/83	Doushantuo@1	580	15.0 ± 0.2‰	16.4	1.4
	Doushantuo@02			24.7	1.2
	Doushantuo@03			21.6	1.5
	Doushantuo@04			14.6	2.2
	Doushantuo@05			19.7	1.7
	Doushantuo@06			21.3	1.3
	Doushantuo@07			14.0	0.9
	Doushantuo@08			20.1	1.0
	Doushantuo@09			14.5	0.9
	Doushantuo@10			17.3	1.3
	Doushantuo@11			9.2	0.8
	Doushantuo@12			15.1	1.0
	Doushantuo@15			13.1	1.0
Bitter Springs 3 of 11/2/90	Bitter@02	800		6.6	1.0
	Bitter@05			10.7	1.4
	Bitter@07			17.0	1.2
	Bitter@08			11.7	0.8
	Bitter@10			5.6	0.9
	Bitter@12			2.5	0.9
	Bitter@13			2.0	1.0
	Bitter@15			8.1	1.0
	Bitter@16			10.9	1.0
	Bitter@17			3.4	0.9
	Bitter@18			10.0	1.0
	Bitter@19			12.4	0.9
	Bitter@21			9.9	1.1
	Bitter@22			7.8	1.1
	Bitter@23			16.1	0.8
	Bitter@24			5.7	1.3
	Bitter@25			11.5	1.1
	Bitter@26			9.3	0.8
	Bitter@30			6.6	1.0
	Bitter@32			13.0	1.0
	Bitter@33			4.2	1.2
	Bitter@34			5.1	1.0
	Bitter@35			10.4	0.8
	Bitter@37			8.8	1.0

Sample	Analysis Name	Age (Ma)	Bulk $\delta^{18}O$ (‰)	$\delta^{18}O$ corr. IMF (‰)	2σ (‰)
	Bitter@38			12.1	1.1
	Bitter@42			6.1	1.1
	Bitter@43			6.7	1.3
	Bitter@44			8.4	1.0
	Bitter@47			6.6	0.9
	Bitter@50			10.3	1.1
Jixian 1 of 8/14/83	Jixian@05	1500		21.7	1.0
	Jixian@08			22.1	1.1
	Jixian@09			30.9	0.8
	Jixian@10			28.7	1.0
	Jixian@13			25.9	1.0
	Jixian@19			28.9	0.9
	Jixian@20			32.4	1.2
	Jixian@21			30.4	1.0
	Jixian@22			33.1	0.9
	Jixian@23			28.5	0.9
	Jixian@26			28.2	1.0
	Jixian@27			30.0	0.9
	Jixian@28			28.7	0.9
	Jixian@32			26.9	0.8
	Jixian@33			28.3	0.9
	Jixian@34			31.4	0.9
	Jixian@35			27.8	0.9
McArthur 7 of 6/21/90	McArthur@1	1600		27.1	0.8
	McArthur@02			22.7	1.0
	McArthur@03			29.1	0.8
	McArthur@04			24.1	0.9
	McArthur@05			25.8	0.9
	McArthur@09			24.3	0.9
	McArthur@12			27.3	0.9
	McArthur@13			16.7	1.0
	McArthur@14			19.4	1.0
	McArthur@15			27.1	1.0
	McArthur@16			20.5	0.9
	McArthur@23			23.0	0.9
	McArthur@24			29.6	0.9
Gunflint 3 of 6/30/84	Gunflint@126	1880	7.3 ± 1.0‰	4.6	1.4
	Gunflint@127			3.8	1.1

Sample	Analysis Name	Age (Ma)	Bulk $\delta^{18}O$ (‰)	$\delta^{18}O$ corr. IMF (‰)	2σ (‰)
	Gunflint@128			4.2	0.9
	Gunflint@129			9.2	0.9
	Gunflint@131			3.9	1.4
	Gunflint@133			2.6	2.5
	Gunflint@134			2.7	1.1
Gunflint PPRG 134	PPRG134@02			-2.5	1.9
	PPRG134@09			2.0	2.5
	PPRG134@11			4.5	2.3
	PPRG134@12			4.1	2.1
	PPRG134@13			6.3	2.0
	PPRG134@15			4.5	2.1
	PPRG134@18			6.4	2.3
	PPRG134@25			4.6	2.5
	PPRG134@26			5.7	2.4
	PPRG134@27			2.2	2.3
	PPRG134@29			9.3	3.1
	PPRG134@32			7.7	2.2
	PPRG134@33			1.7	2.5
	PPRG134@35			0.4	2.4
	PPRG134@37			0.6	2.0
	PPRG134@39			1.8	2.3
	PPRG134@42			10.6	3.1
Nabberu PPRG 089	Naberu@02	1850		21.2	2.5
	Naberu@06			22.4	2.5
	Naberu@08			17.2	2.1
	Naberu@09			26.1	3.1
	Naberu@10			28.8	2.2
	Naberu@14			17.8	2.3
	Naberu@15			28.3	1.9
	Naberu@16			32.0	3.1
	Naberu@18			33.3	2.4
	Naberu@19			16.1	1.7
	Naberu@20			23.6	2.0
	Naberu@23			26.7	2.5
	Naberu@24			31.0	1.8
	Naberu@25			25.3	3.0
Wabigoon PPRG 325	Wabigoon@1	2700		26.2	0.9
	Wabigoon@03			19.4	1.5

Sample	Analysis Name	Age (Ma)	Bulk $\delta^{18}O$ (‰)	$\delta^{18}O$ corr. IMF (‰)	2σ (‰)
	Wabigoon@04			28.5	0.9
	Wabigoon@17			31.6	0.9
	Wabigoon@19			24.2	0.9
	Wabigoon@20			26.5	0.9
	Wabigoon@21			30.3	0.8
	Wabigoon@23			27.9	0.9
	Wabigoon@26			33.3	0.9
	Wabigoon@29			28.6	0.9
	Wabigoon@31			28.5	0.9
Farrel Quartzite MGTKS1	MGTKS1@50	3020	19.8 ± 0.1 ‰	18.3	0.7
	MGTKS1@51			22.0	0.7
	MGTKS1@53			21.1	0.9
	MGTKS1@54			18.9	0.7
	MGTKS1@55			13.2	0.9
	MGTKS1@56			17.0	0.8
	MGTKS1@57			17.2	0.7
	MGTKS1@58			20.7	0.6
	MGTKS1@60			20.1	0.6
	MGTKS1@61			22.3	0.6
	MGTKS1@64			22.9	0.6
	MGTKS1@65			20.7	0.6
	MGTKS1@66			23.4	0.6
	MGTKS1@68			27.8	0.5
	MGTKS1@70			20.7	0.9
	MGTKS1@71			23.4	0.7
	MGTKS1@73			15.6	1.2
	MGTKS1@74			21.2	0.8
	MGTKS1@77			22.5	0.6
	MGTKS1@78			24.1	0.6
	MGTKS1@79			24.1	0.8
	MGTKS1@81			16.9	0.7
	MGTKS1@82			15.7	0.6
	MGTKS1@83			19.6	0.6
	MGTKS1@85			17.6	0.8
	MGTKS1@86			25.9	0.5
	MGTKS1@88			19.7	0.6
	MGTKS1@89			23.9	0.5

Sample	Analysis Name	Age (Ma)	Bulk $\delta^{18}O$ (‰)	$\delta^{18}O$ corr. IMF (‰)	2σ (‰)
	MGTKS1@02			25.5	2.1
	MGTKS1@04			22.0	2.0
	MGTKS1@05			27.9	1.9
	MGTKS1@07			26.0	2.0
	MGTKS1@08			26.4	2.2
	MGTKS1@10			23.9	2.1
	MGTKS1@14			28.3	2.3
	MGTKS1@17			31.6	2.1
	MGTKS1@18			28.1	2.0
	MGTKS1@21			20.6	2.4
	MGTKS1@22			25.9	1.9
	MGTKS1@23			22.0	1.9
	MGTKS1@27			26.6	2.0
	MGTKS1@28			25.2	2.1
	MGTKS1@29			25.6	2.0
	MGTKS1@30			22.1	2.0
	MGTKS1@32			24.2	2.3
	MGTKS1@33			26.7	2.0
	MGTKS1@34			23.7	2.2
	MGTKS1@40			25.1	2.0
	MGTKS1@42			26.9	2.0
Josefsdal 99SA07	Josefsdal@02	3300		21.7	1.9
	Josefsdal@05			22.4	1.9
	Josefsdal@06			21.2	1.9
	Josefsdal@07			22.5	1.9
	Josefsdal@10			21.6	1.9
	Josefsdal@11			21.0	1.9
	Josefsdal@14			20.8	1.9
	Josefsdal@16			21.0	1.9
	Josefsdal@18			21.5	1.9
	Josefsdal@19			19.6	1.9
	Josefsdal@23			22.6	1.9
	Josefsdal@25			23.9	1.9
	Josefsdal@26			22.7	1.9
	Josefsdal@27			22.3	1.9
	Josefsdal@28			21.3	1.9
	Josefsdal@29			23.1	1.9

Sample	Analysis Name	Age (Ma)	Bulk $\delta^{18}O$ (‰)	$\delta^{18}O$ corr. IMF (‰)	2σ (‰)
Buck Reef 99SA03	Buck@03	3420	15.0 ± 0.7‰	19.7	2.5
	Buck@05			18.7	1.5
	Buck@06			24.8	1.6
	Buck@07			19.1	1.6
	Buck@08			21.2	0.8
	Buck@13			20.5	1.4
	Buck@14			16.4	1.2
	Buck@16			19.1	2.0
	Buck@18			17.5	1.8
	Buck@20			20.3	2.2
	Buck@21			15.9	1.8
	Buck@22			21.0	1.4
	Buck@23			18.2	1.8
	Buck@26			17.4	2.1
	Buck@27			28.4	1.1
	Buck@28			23.3	1.7
	Buck@31			17.5	1.2
	Buck@33			16.1	1.5
	Buck@34			17.5	2.3
	Buck@36			17.2	2.1

Supplementary Information References

Akin, S.J., Pufahl, P.K., Hiatt, E.E., Pirajno, F. (2013) Oxygenation of shallow marine environments and chemical sedimentation in Palaeoproterozoic peritidal settings: Frere Formation, Western Australia. *Sedimentology* 60, 1559-1582.

Alleon, J., Bernard, S., Le Guillou, C., Marin-Carbonne, J., Pont, S., Beyssac, O., McKeegan, K.D., Robert, F. (2016) Molecular preservation of 1.88 Ga Gunflint organic microfossils as a function of temperature and mineralogy. *Nature Communications* 7, 11977.

Awramik, S.M., Barghoorn, E.S. (1977) Gunflint Microbiota. *Precambrian Research* 5, 121-142.

Awramik, S.M., McMenamin, D.S., Chongyu, Y., Ziqiang, Z., Qixiu, D., Shusen, Z. (1985) Prokaryotic and eukaryotic microfossils from a Proterozoic/Phanerozoic transition in China. *Nature* 315, 655-658.

Barghoorn, E.S., Schopf, J.W. (1965) Microorganisms from the Late Precambrian of central Australia. *Science* 150, 337-339.

Barghoorn, E.S., Tyler, S.A. (1965) Microorganisms from the Gunflint chert. *Science* 147, 563-575.

Beaumont, V., Robert, F. (1999) Nitrogen isotope ratios of kerogens in Precambrian cherts: a record of the evolution of atmosphere chemistry? *Precambrian Research* 96, 63-82.

Carrigan, W.J., Cameron, E.M. (1991) Petrological and stable isotope studies of carbonate and sulphide minerals from the Gunflint Formation, Ontario: evidence for the origin of early Proterozoic iron-formation. *Precambrian Research* 52, 347-380.

Charnay, B. (2014) Dynamique troposphérique et évolution climatique de Titan et de la Terre primitive. Ph.D. thesis, Université Pierre et Marie Curie – Paris VI, 240 pp. Available at https://tel.archives-ouvertes.fr/tel-00987546/document.

Charnay, B., Forget, F., Wordsworth, R., Leconte, J., Millour, E., Codron, F., Spiga, A. (2013) Exploring the faint young Sun problem and the possible climates of the Archean Earth with a 3-D GCM. *Journal of Geophysical Research: Atmospheres* 118, 10,414-10,431.

Cheng, J.B., Zhang, H.M., Xing, Y.S., Ma, G.G. (1981) On the Upper Precambrian (Sinian Suberathem) in China. *Precambrian Research* 15, 207-228.

Cloud, P.E. (1965) The significance of the Gunflint (Precambrian) microflora. *Science* 148, 27-35.

Condon, D.J., Zhu, M., Bowring, S.A., Wang, W., Yang, A., Jin, Y. (2005) U-Pb ages from the Neoproterozoic Doushantuo Formation, China. *Science* 308, 95-98.

Durand, B., Monin, J.C. (1980) Elemental analysis of kerogens (C, H, O, N, S, Fe). In: Durand, B. (Ed.) *Kerogen – Insoluble organic matter from sedimentary rocks.* Technip, Paris, France, 113-142.

Durand, B., Nicaise, G. (1980) Procedures for kerogen isolation. In: Durand, B. (Ed.) *Kerogen – Insoluble organic matter from sedimentary rocks.* Technip, Paris, France, 35-54.

Fralick, P.W., Davis, D.W., Kissin, S.A. (2002) The age of the Gunflint Formation, Ontario, Canada: single zircon U-Pb age determinations from reworked volcanic ash. *Canadian Journal of Earth Sciences* 39, 1085-1091.

Fralick, P.W., Riding, R. (2015) Steep Rock Lake: Sedimentology and geochemistry of an Archean carbonate platform. *Earth-Science Reviews* 151, 132-175.

Grey, K., Sugitani, K. (2009) Palynology of Archean microfossils (c. 3.0 Ga) from the Mount Grant area, Pilbara Craton, Western Australia: Further evidence of biogenicity. *Precambrian Research* 173, 60-69.

Guo, Q., Liu, C., Strauss, H., Goldberg, T., Zhu, M., Pi, D., Wang, J. (2006) Organic carbon isotope geochemistry of the Neoproterozoic Doushantuo Formation, South China. *Acta Geologica Sinica* 80, 670-683.

Hayes, J.M., Kaplan, I.R., Wedeking, K.W. (1983) Precambrian Organic Geochemistry, Preservation of the Record. In: Schopf, J.W. (Ed.) *Earth's Earliest Biosphere. Its Origin and Evolution.* Princeton University Press, Princeton, NJ, 93-134.

Hill, A.C., Walter, M.R. (2000) Mid-Neoproterozoic (~830-750 Ma) isotope stratigraphy of Australia and global correlation. *Precambrian Research* 100, 181-211.

Hill, A.C., Arouri, K., Gorjan, P., Walter, M.R. (2000) Geochemistry of marine and nonmarine environments of a Neoproterozoic cratonic carbonate/evaporate: The Bitter Springs Formation, central Australia. In: Grotzinger, J.P., James, N.P. (Eds.) *Carbonate Sedimentation and Diagenesis in the Evolving Precambrian World.* Society of Economic Paleontologists and Mineralogists Special Publication 67, Tulsa, OK, 327-344.

House, C.H., Oehler, D.Z., Sugitani, K., Mimura, K. (2013) Carbon isotopic analyses of *ca.* 3.0 Ga microstructures imply planktonic autotrophs inhabited Earth's early oceans. *Geology* 41, 651-654.

Hren, M.T., Tice, M.M., Chamberlain, C.P. (2009) Oxygen and hydrogen isotope evidence for a temperate climate 3.42 billion years ago. *Nature* 462, 205-208.

Jaffrés, J.B.D., Shields, G.A., Wallmann, K. (2007) The oxygen isotope evolution of seawater: A critical review of a long-standing controversy and an improved geological water cycle model for the past 3.4 billion years. *Earth-Science Reviews* 83, 83-122.

Kasting, J.F., Howard, M.T., Wallmann, K., Veizer, J., Shields, G.A., Jaffrés, J.B.D. (2006) Paleoclimates, ocean depth, and the oxygen isotopic composition of seawater. *Earth and Planetary Science Letters* 252, 82-93.

Knauth, L.P. (2005) Temperature and salinity history of the Precambrian ocean: Implications for the course of microbial evolution. *Palaeogeography, Palaeoclimatology, Palaeoecology* 219, 53-69.

Knauth, L.P., Epstein, S. (1976) Hydrogen and oxygen isotope ratios in nodular and bedded cherts. *Geochimica et Cosmochimica Acta* 40, 1095-1108.

Knauth, L.P., Lowe, D.R. (1978) Oxygen isotope geochemistry of cherts from Onverwacht group (3.4 Billion Years), Transvaal, South-Africa, with implications for secular variations in isotopic composition of cherts. *Earth and Planetary Science Letters* 41, 209-222.

Knauth, L.P., Lowe, D.R. (2003) High Archean climatic temperature inferred from oxygen isotope geochemistry of cherts in the 3.5 Ga Swaziland Supergroup, South Africa. *Geological Society of America Bulletin* 115, 566-580.

Kreuzer-Martin, H.W., Jarman, K.H. (2007) Stable isotope ratios and forensic analysis of microorganisms. *Applied Environmental Microbiology* 73, 3896-3908.

Li, H.K., Zhu, S.X., Xiang, Z.Q., Su, W.B., Lu, S.N., Zhou, H.Y., Geng, J.Z., Li, S., Yang, F.J. (2010) Zircon U-Pb dating on tuff bed from Gaoyuzhuang Formation in Yanqing, Beijing: Further constraints on the new subdivision of the Mesoproterozoic stratigraphy in the North China Craton. *Acta Petrologica Sinica* 26, 2131-2140.

Lindsay, J.F., Kruse, P.D., Green, O.R., Hawkins, E., Brasier, M.D., Cartlidge, J., Corfield, R.M. (2005) The Neoproterozoic-Cambrian record in Australia: A stable isotope study. *Precambrian Research* 143, 113-133.

Lu, S., Zhao, G., Wang, H., Hao, G. (2008) Precambrian metamorphic basement and sedimentary cover of the North China Craton: A review. *Precambrian Research* 160, 77-93.

Marin, J., Chaussidon, M., Robert, F. (2010) Microscale oxygen isotope variations in 1.9 Ga Gunflint cherts: Assessments of diagenesis effects and implications for oceanic paleotemperature reconstructions. *Geochimica et Cosmochimica Acta* 74, 116-130.

Mayr, C., Laprida, C., Lücke, A., Martín, R.S., Massaferro, J., Ramón-Mercau, J., Wissel, H. (2015) Oxygen isotope ratios of chironomids, aquatic macrophytes and ostracods for lakewater isotopic reconstructions - Results of a calibration study in Patagonia. *Journal of Hydrology* 529, 600-607.

Muir, M.D. (1976) Proterozoic microfossils from the Amelia Dolomite, McArthur Basin, Northern Territory. *Alcheringa* 1, 143-158.

Oehler, D.Z. (1978) Microflora of the middle Proterozoic Balbirini Dolomite (McArthur Group) of Australia. *Alcheringa* 2, 269-309.

Oehler, D.Z., Robert, F., Walter, M.R., Sugitani, K., Allwood, A., Meibom, A., Mostefaoui, S., Selo, M., Thomen, A., Gibson, E.K. (2009) NanoSIMS: Insights to biogenicity and syngeneity of Archaean carbonaceous structures. *Precambrian Research* 173, 70-78.

Perry Jr., E.C. (1967) The oxygen isotopic chemistry of ancient cherts. *Earth and Planetary Science Letters* 3, 62-66.

Pesonen, L.J., Mertanen, S., Veikkolainen, T. (2012) Paleo-Mesoproterozoic Supercontinents – A Paleomagnetic View. *Geophysica* 48, 5-47.

Pirajno, F., Hocking, R.M., Reddy, S.M., Jones, A.J. (2009) A review of the geology and geodynamic evolution of the Paleoproterozoic Earaheedy Basin, Western Australia. *Earth-Science Reviews* 94, 39-77.

Rasmussen, B., Fletcher, I.R., Bekker, A., Muhling, J.R., Gregory, C.J., Thorne, A.M. (2012) Deposition of 1.88-billion-year-old iron formations as a consequence of rapid crustal growth. *Nature* 484, 498-501.

Rawlings, D.J. (1999) Stratigraphic resolution of a multiphase intracratonic basin system: the McArthur Basin, northern Australia. *Australian Journal of Earth Sciences* 46, 703-723.

Robert, F., Chaussidon, M. (2006) A palaeo-temperature curve for the Precambrian oceans based on silicon isotopes in cherts. *Nature* 443, 969-972.

Sangély, L., Chaussidon, M., Michels, R., Huault, V. (2005) Microanalysis of carbon isotope composition in organic matter by secondary ion mass spectrometry. *Chemical Geology* 223, 179-195.

Schopf, J.W. (1968) Microflora of the Bitter Springs Formation, Late Precambrian, Central Australia. *Journal of Paleontology* 42, 651-688.

Schopf, J.W., Zhu, W.Q., Xu, Z.L., Hsu, J. (1984) Proterozoic stromatolitic microbiotas of the 1400-1500 Ma-old Gaoyuzhuang Formation near Jixian, Northern China. *Precambrian Research* 24, 335-349.

Schulz, K.J., Cannon, W.F. (2007) The Penokean orogeny in the Lake Superior region. *Precambrian Research* 157, 4-25.

Soto, D.X., Wassenaar, L.I., Hobson, K.A. (2013) Stable hydrogen and oxygen isotopes in aquatic food webs are tracers of diet and provenance. *Functional Ecology* 27, 535-543.

Strauss, H., Moore, T.B. (1992) Abundances and Isotopic Compositions of Carbon and Sulfur Specie Species in Whole Rock and kerogen Samples. In: Schopf, J.W., Klein, C. (Eds.) *The Proterozoic Biosphere – A Multidisciplinary Study*. Cambridge University Press, Cambridge, NY, 709-798.

Sugahara, H., Sugitani, K., Mimura, K., Yamashita, F., Yamamoto, K. (2010) A systematic rare-earth elements and yttrium study of Archean cherts at the Mount Goldsworthy greenstone belt in the Pilbara Craton: Implications for the origin of microfossil-bearing black cherts. *Precambrian Research* 177, 73-87.

Sugitani, K., Grey, K., Allwood, A., Nagaoka, T., Mimura, K., Minami, M., Marshall, C.P., Van Kranendonk, M.J., Walter, M.R. (2007) Diverse microstructures from Archaean chert from the Mount Goldsworthy-Mount Grant area, Pilbara Craton, Western Australia: Microfossils, dubiofossils, or pseudofossils? *Precambrian Research* 158, 228-262.

Sugitani, K., Grey, K., Nagaoka, T., Mimura, K. (2009) Three-dimensional morphological and textural complexity of Archean putative microfossils from the Northeastern Pilbara Craton: Indications of biogenicity of large (> 15 μm) spheroidal and spindle-like structures. *Astrobiology* 9, 603-615.

Tartèse, R., Chaussidon, M., Gurenko, A., Delarue, F., Robert, F. (2016) *In situ* oxygen isotope analysis of fossil organic matter. *Geochimica et Cosmochimica Acta* 182, 24-39.

Tice, M.M. (2009) Environmental controls on photosynthetic microbial mat distribution and morphogenesis on a 3.42 Ga clastic-starved platform. *Astrobiology* 9, 989-1000.

Tice, M.M., Lowe, D.R. (2004) Photosynthetic microbial mats in the 3,416-Myr-old ocean. *Nature* 431, 549-552.

Tice, M.M., Lowe, D.R. (2006) The origin of carbonaceous matter in pre-3.0 Ga greenstone terrains: a review and new evidence from the 3.42 Ga Buck Reef chert. *Earth-Science Reviews* 76, 259-300.

Tobin, K.J. (1990) The paleoecology and significance of the Gunflint-type microbial assemblages from the Frere Formation (Early Proterozoic), Nabberu Basin, Western Australia. *Precambrian Research* 47, 71-81.

Van Kranendonk, M.J., Smithies, R.H., Hickman, A.H., Champion, D.C. (2007) Secular tectonic evolution of Archean continental crust: Interplay between horizontal and vertical processes in the formation of the Pilbara Craton, Australia. *Terra Nova* 19, 1-38.

Walter, M.R., Goode, A.D.T., Hall, W.D.M. (1976) Microfossils from a newly discovered Precambrian stromatolitic iron formation in Western Australia. *Nature* 261, 221-223.

Walter, M.R., Hofmann, H.J., Schopf, J.W. (1983) Geographic and geological data for processed rock samples. In: Schopf, J.W. (Ed.) *Earth's Earliest Biosphere. Its Origin and Evolution*. Princeton University Press, Princeton, NJ, 385-413.

Wang, Y.V., O'Brien, D.M., Jenson, J., Francis, D., Wooller, M.J. (2009) The influence of diet and water on the stable oxygen and hydrogen isotope composition of Chironomidae (Diptera) with paleoecological implications. *Oecologia* 160, 225-233.

Wedeking, K.W. (1983) The Biogeochemistry of Precambrian Kerogen. Ph.D. thesis, Indiana University, 167 pp.

Wedeking, K.W., Hayes, J.M. (1983) Exchange of oxygen isotopes between water and organic material. *Chemical Geology* **1**, 357-370.

Westall, F., de Wit, M.J., Dann, J., van der Gaast, S., de Ronde, C.E.J., Gerneke, D. (2001) Early Archean fossil bacteria and biofilms in hydrothermally-influenced sediments from the Barberton greenstone belt, South Africa. *Precambrian Research* 106, 93-116.

Westall, F., de Ronde, C.E.J., Southam, G., Grassineau, N., Colas, M., Cockell, C., Lammer, H. (2006) Implications of a 3.472-3.333 Ga old subaerial microbial mat from the Barberton Greenstone Belt, South Africa for the UV environmental conditions on the early Earth. *Philosophical Transactions of the Royal Society B* 361, 1857-1876.

Westall, F., Cavalazzi, B., Laurence, L., Marrocchi, Y., Rouzaud, J.-N., Simionovici, A., Salome, G., MacLean, L., Wirick, S., Hofmann, A., Meibom, A., Robert, F., Defarge, C. (2011) Implications of *in situ* calcification for photosynthesis in a ~3.3 Ga-old microbial biofilm from the Barberton greenstone belt, South Africa. *Earth and Planetary Science Letters* 310, 468-479.

Westall, F., Campbell, K.A., Bréhéret, J.G., Foucher, F., Gautret, P., Hubert, A., Sorieul, S., Grassineau, N., Guido, D.M. (2015) Archean (3.33 Ga) microbe-sediment systems were diverse and flourished in a hydrothermal context. *Geology* 43, 615-618.

Wilks, M.E., Nisbet, E.G. (1985) Archaean stromatolites from the Steep Rock Group, northwestern Ontario, Canada. *Canadian Journal of Earth Sciences* 22, 792-799.

Wilks, M.E., Nisbet, E.G. (1988) Stratigraphy of the Steep Rock Group, northwest Ontario: a major Archaean unconformity and Archaean stromatolites. *Canadian Journal of Earth Sciences* 25, 370-391.

Winter, B.L., Knauth, L.P. (1992) Stable isotope geochemistry of cherts and carbonates from the 2.0-Ga Gunflint iron formation – implications for the depositional setting, and the effects of diagenesis and metamorphism. *Precambrian Research* 59, 283-313.

Xu, L.Z., Awramik, S.M. (2002) The Gaoyuzhuang Palaeobiology. *Acta Botanica Sinica* 44, 617-627.

Zech, M., Werner, R.A., Juchelka, D., Kalbitz, K., Buggle, B., Glaser, B. (2012) Absence of oxygen isotope fractionation/exchange of (hemi-) cellulose derived sugars during litter decomposition. *Organic Geochemistry* 42, 1470-1475.

Zhang, Y. (1981) Proterozoic stromatolite microfloras of the Gaoyuzhuang Formation (Early Sinian: Riphean), Hebei, China. *Journal of Paleontology* 55, 485-506.

Zhang, S., Jiang, G., Zhang, J., Song, B., Kennedy, M.J., Christie-Blick, N. (2005) U-Pb sensitive high-resolution ion microprobe ages from the Doushantuo Formation in south China: Constraints on late Neoproterozoic glaciations. *Geology* 33, 473-476.